PHILOSOPHICAL TRANSACTIONS OF THE ROYAL SOCIETY A MATHEMATICAL, PHYSICAL & ENGINEERING SCIENCES

Structure, Chemical Mechanism and Properties of Premixed Flames in Mixtures of Carbon Monoxide, Nitrogen and Oxygen with Hydrogen and Water Vapour

M. A. Cherian, P. Rhodes, R. J. Simpson and G. Dixon-Lewis

Phil. Trans. R. Soc. Lond. A 1981 **303**, 181-212
doi: 10.1098/rsta.1981.0196

Phil. Trans. R. Soc. Lond. A **303**, 181–212 (1981) [181]
Printed in Great Britain

STRUCTURE, CHEMICAL MECHANISM AND PROPERTIES OF PREMIXED FLAMES IN MIXTURES OF CARBON MONOXIDE, NITROGEN AND OXYGEN WITH HYDROGEN AND WATER VAPOUR

By M. A. Cherian, P. Rhodes, R. J. Simpson† and G. Dixon-Lewis

Department of Fuel and Energy, The University, Leeds LS2 9JT, U.K.

(*Communicated by P. Gray, F.R.S. – Received 29 April* 1981)

CONTENTS

PAGE

1. Introduction 183

2. Computational procedures and input data 184
   (*a*) General outline 184
   (*b*) Transport property calculations 185
   (*c*) Reaction rate coefficients and equilibrium constants 186

3. Results 188
   (*a*) Addition of small amounts of carbon monoxide to a low temperature, fuel-rich hydrogen–oxygen–nitrogen flame 188
   (*b*) Addition of a trace of carbon dioxide to gases entering a low temperature hydrogen–oxygen–nitrogen flame 191
   (*c*) Addition of carbon monoxide to a low temperature hydrogen–oxygen–argon flame 191
   (*d*) Burning velocities of hydrogen–carbon monoxide–air flames at atmospheric pressure 192
   (*e*) Flames in carbon monoxide–air mixtures containing traces of hydrogen or water vapour, or both 195
   (*f*) Structures of two hydrogen–carbon monoxide–oxygen flames at reduced pressure 196

4. Discussion 199
   (*a*) Flame mechanism 199
   (*b*) Reaction rate parameters 210

References 211

† Present address: British Gas Corporation, Research and Development Division, Watson House, Peterborough Road, London SW6 3HN, U.K.

Vol. 303. A 1476. 18 [Published 26 November 1981

Implicit solutions of the time-dependent flame equations have been used to calculate, for assumed reaction mechanisms, the expected structures and properties of a series of hydrogen–carbon monoxide–oxygen–nitrogen flames, some containing traces of added water vapour, at atmospheric and reduced pressures. Predicted burning velocities at atmospheric pressure have been compared with:

(*a*) recent measurements, reported here, of the effect of addition of up to 10 % carbon monoxide on the burning velocity of a low temperature hydrogen–oxygen–nitrogen flame;

(*b*) previous measurements by Scholte & Vaags (1959*c*) on dry hydrogen–carbon monoxide–air mixtures over the whole composition range on the fuel-rich side of stoichiometric; and

(*c*) previously reported measurements by Jahn (1934), Badami & Egerton (1955), Scholte & Vaags (1959*b*) and Wires *et al.* (1959) for moist carbon monoxide–air or carbon monoxide–oxygen mixtures, with or without traces of added hydrogen.

Additionally, the following comparisons are made:

(*d*) The mole fraction profile for the decay of a trace of carbon dioxide added to the low temperature hydrogen–oxygen–nitrogen flame has been recalculated with the aid of the full reaction mechanism, for comparison with the previously reported measurements of Dixon-Lewis *et al.* (1965).

(*e*) Computed structures of two hydrogen–carbon monoxide–oxygen–argon flames burning at reduced pressure have been compared with previous measurements by Fenimore & Jones (1959) and Vandooren *et al.* (1975).

(*f*) The mole fraction ratio X_{CO}/X_{CO_2} in the burnt gas from a low temperature, fuel-rich hydrogen–carbon monoxide–oxygen–argon flame at atmospheric pressure was measured by using a mass spectrometer. The measured ratio agreed to within 1 % with that predicted by computation of the complete flame properties. Both the calculated and measured ratios were higher than would correspond with the establishment of the water gas equilibrium in the flame.

The major part of the observed changes in burning velocity from those of hydrogen–air mixtures can be satisfactorily explained by the addition of the single reaction (xxi),

$$OH + CO \rightleftharpoons CO_2 + H, \qquad \text{(xxi)}$$

to the mechanism already established for the hydrogen–oxygen–nitrogen flame system (Dixon-Lewis 1979). This applies particularly to fuel-lean flames and to fuel-rich mixtures not too far from stoichiometric. For fuel-rich flames further from stoichiometric, and particularly for the measurements in §(a), agreement between predicted and measured burning velocities is improved by adding to the mechanism a series of chain terminating steps involving the formation and subsequent reactions of the formyl radical. For reasonable values of its rate coefficient, reaction (xxii),

$$O + CO + M \rightleftharpoons CO_2 + M, \qquad \text{(xxii)}$$

never exerts more than a minor influence on the burning velocity.

The major features of the structure of the flames are:

(*a*) a preferential oxidation of hydrogen in the early stages of the reaction zones, leading to overshoot in the water concentration followed by a slow approach to the water gas equilibrium from the carbon monoxide–water side; and

(*b*) marked enrichment of the oxygen atom concentration in the radical pool as the hydrogen content of the flames is decreased. In the flames containing only traces of hydrogen, the degree of enrichment is markedly influenced by reaction (xxii).

1. Introduction

Carbon monoxide and hydrogen are both important intermediate compounds in the high temperature flame oxidation of hydrocarbons. Early studies of the structure of fuel-lean flames of hydrocarbons burning in air first demonstrated the two stage nature of the oxidation mechanism (Friedman & Burke 1954; Prescott *et al.* 1954; Friedman & Cyphers 1955; Fristrom & Westenberg 1957). The first stage consisted of the rapid oxidation of the hydrocarbon principally to carbon monoxide and water vapour, with some hydrogen also formed. The second stage, the oxidation of the carbon monoxide to carbon dioxide, was slower, and took place over a more extended region on the hot, burnt gas side of the flame. The reaction responsible for the bulk of the slow oxidation to carbon dioxide is the forward reaction (xxi):

$$OH + CO \rightleftharpoons CO_2 + H. \qquad \text{(xxi)}$$

Many studies of this reaction, by a variety of experimental techniques, have led to the mean rate expression $k_{21} = 1.5 \times 10^7\ T^{1.3} \exp(+385/T)\ \text{cm}^3\ \text{mol}^{-1}\ \text{s}^{-1}$ between 250 and 2000 K, with suggested error limits of $\pm 50\,\%$ (Baulch & Drysdale 1974).

Besides reaction (xxi), carbon monoxide may undergo two further reactions with the chain carriers of the hydrogen–oxygen system. These are

$$O + CO + M \rightleftharpoons CO_2 + M, \qquad \text{(xxii)}$$

$$H + CO + M \rightleftharpoons HCO + M. \qquad \text{(xxiii)}$$

Reaction (xxii) has been used by Buckler & Norrish (1938), Dixon-Lewis & Linnett (1953), and Baldwin *et al.* (1972) to explain the main features of the effect of carbon monoxide on the second explosion limit of the hydrogen–oxygen system. Baldwin *et al.* (1972) have also found it necessary to invoke reaction (xxiii) when analysing the same data. Reactions (xxii) and (xxiii) are much slower than reaction (xxi), so that reaction (xxi) alone is responsible for the bulk of the oxidation of the carbon monoxide in flames and other systems. The importance of reactions (xxii) and (xxiii) lies in their chain-terminating capabilities, which affect the overall concentration of chain carriers. In hydrogen–carbon monoxide–oxygen flame systems the formyl radical formed in reaction (xxiii) will either redissociate by reaction (−xxiii) or undergo one of the forward reactions (xxiv) to (xxvii):

$$HCO + O_2 \rightleftharpoons HO_2 + CO, \qquad \text{(xxiv)}$$

$$HCO + H \rightleftharpoons H_2 + CO, \qquad \text{(xxv)}$$

$$HCO + OH \rightleftharpoons H_2O + CO, \qquad \text{(xxvi)}$$

$$HCO + O \rightleftharpoons OH + CO. \qquad \text{(xxvii)}$$

All these reactions of the formyl radical are important also in the flame oxidation of methane and other hydrocarbons, since one of the principal routes to carbon monoxide in such flames is via formaldehyde and the formyl radical. Compared with hydrogen–oxygen flames, studies of the hydrogen–carbon monoxide–oxygen or hydrogen–carbon monoxide–air flame systems may therefore provide information about an important further subgroup of the reactions

PHILOSOPHICAL TRANSACTIONS OF THE ROYAL SOCIETY A MATHEMATICAL, PHYSICAL & ENGINEERING SCIENCES

involved in the hydrocarbon flames. An investigation of these reactions is the object of the present work.

The investigation started from the reaction mechanism and mean rate parameters already established for hydrogen–oxygen–nitrogen flames (Dixon-Lewis 1979). This mechanism, with the new reactions (xxi) to (xxvii) also incorporated, was used to calculate the burning velocities of a wide range of premixed hydrogen–carbon monoxide–oxygen–nitrogen, hydrogen–carbon monoxide–air and moist carbon monoxide–air flames, for comparison with experiment. The computations required the assignment of rate parameters to each of the new elementary processes. The comparison with experiment was used, as far as possible, to derive information about the new rate parameters, so as to produce a satisfactory model for the flames.

2. Computational procedures and input data

(*a*) *General outline*

With the addition of reactions (xxi) to (xxvii) inclusive to the established mechanism for hydrogen–oxygen supported flames (Dixon-Lewis 1979), the complete set of reactions controlling the carbon monoxide containing system becomes:

	ΔH°_{298}/(kJ mol^{-1}) (forward reaction)	
$OH + H_2 \rightleftharpoons H_2O + H$	−63.30	(i)
$H + O_2 \rightleftharpoons OH + O$	+70.67	(ii)
$O + H_2 \rightleftharpoons OH + H$	+8.26	(iii)
$H + O_2 + M \rightleftharpoons HO_2 + M$	−197.07	(iv)
$H + HO_2 \rightleftharpoons OH + OH$	−159.98	(vii)
$H + HO_2 \rightleftharpoons O + H_2O$	−231.54	(vii*a*)
$H + HO_2 \rightleftharpoons H_2 + O_2$	−238.91	(xii)
$OH + HO_2 \rightleftharpoons H_2O + O_2$	−302.21	(xiii)
$O + HO_2 \rightleftharpoons OH + O_2$	−230.65	(xiv)
$H + H + M \rightleftharpoons H_2 + M$	−435.97	(xv)
$H + OH + M \rightleftharpoons H_2O + M$	−499.28	(xvi)
$H + O + M \rightleftharpoons OH + M$	−427.72	(xvii)
$OH + OH \rightleftharpoons O + H_2O$	−71.56	(xviii)
$OH + CO \rightleftharpoons CO_2 + H$	−104.72	(xxi)
$O + CO + M \rightleftharpoons CO_2 + M$	−532.19	(xxii)
$H + CO + M \rightleftharpoons HCO + M$	−63.94	(xxiii)
$HCO + O_2 \rightleftharpoons HO_2 + CO$	−133.12	(xxiv)
$H + HCO \rightleftharpoons H_2 + CO$	−372.03	(xxv)
$OH + HCO \rightleftharpoons H_2O + CO$	−435.58	(xxvi)
$O + HCO \rightleftharpoons OH + CO$	−363.52	(xxvii)

With nitrogen present as diluent, there are eleven chemical species present, namely H, O, OH, N_2, O_2, H_2, CO, CO_2, H_2O, HO_2 and HCO.

Complete flame profiles were computed by implicit solution of the time-dependent flame equations according to the approach initially developed by Patankar & Spalding (1970) for the prediction of steady, two-dimensional, boundary layer flow, and later modified by Spalding & Stephenson (1971), Spalding *et al.* (1971) and Stephenson & Taylor (1973) to predict unsteady one-dimensional flame propagation. The latter modification has recently been refined by Tsatsaronis (1978) to include detailed transport property calculations, using the equations given by Dixon-Lewis (1968). These are based on the extension of the Chapman–

Enskog kinetic theory to polyatomic gases by Wang Chang *et al.* (1964), and the subsequent development by Monchick & Mason (1961), Mason & Monchick (1962) and Monchick *et al.* (1963, 1965, 1966). The overall approach is capable of handling reaction mechanisms of arbitrary complexity, and in obtaining complete solutions to flame problems it is in this respect superior to the alternative method of solution described by Dixon-Lewis *et al.* (1975), which was based on the stationary flame equations. With increasing mechanistic complexity, the stationary flame method becomes limited by the necessity for precise matching of too many independent working hot boundary values. For the hydrogen–oxygen supported flame system, Dixon-Lewis (1979) has shown that for the same reaction mechanism and rate parameters, and with equivalent formulations of the transport properties, the two methods give identical results.

Most of the flames investigated here are free flames, in the sense that the flame sheet is either not attached to a burner at all, or attached only remotely from the region specifically under consideration. Another class of flame, which has been found to be particularly convenient for structure measurements since it is less prone to aerodynamic disturbance, is the so-called 'burner-stabilized flame' in which the cold boundary of the flame is everywhere in intimate contact with a water-cooled porous plate. Fresh combustible mixture is supplied to the flame through this plate, and heat is abstracted at the cold boundary of the flame at a rate controlled by the entering mass flux, so that the latter becomes an effective non-adiabatic mass burning velocity. Compared with the free flame, the modelling of such burner-stabilized flames requires some modification of the cold boundary conditions of integration. These modifications will be discussed elsewhere. In the present paper they are used in modelling two flames for which structures have been measured by Fenimore & Jones (1959) and Vandooren *et al.* (1975).

In addition to the complete flame properties, species profiles in the burnt gas region of several of the flames to be described were computed on the assumption that reactions (i), (ii), (iii) and (xxi) are equilibrated there. These additional calculations were performed by the appropriate partial equilibrium modification of the composite flux method of Dixon-Lewis *et al.* (1975). Comparison of the resulting profiles with those from the complete flame calculations gives an indication of the rate of achievement of partial equilibrium, and hence of completion of the main combustion reaction.

(*b*) *Transport property calculations*

The extension of the flame calculations to hydrogen–carbon monoxide–nitrogen–oxygen mixtures necessitates consideration of molecular transport processes in a mixture of eleven chemical species. Multicomponent diffusion coefficients were calculated for the complete eleven-component system, according to the equations given by Dixon-Lewis (1968). However, the calculation of the thermal conductivity and the multicomponent thermal diffusion coefficients in an N-component system requires the inversion of a $(3N-M)\times(3N-M)$ matrix, where M is the number of monatomic components. To effect economies in computation, only seven of the eleven components of the mixture were considered in the latter context. These were H, N_2, O_2, H_2, CO, CO_2 and H_2O. Atomic hydrogen was retained with the major components in this part of the calculation since Dixon-Lewis (1979) has shown that thermal diffusion of hydrogen atoms contributes observably to the computed burning velocities of hydrogen–air flames.

Table 1. Lennard-Jones (12:6) potential parameters

species	(eps/k)/K	σ/nm	ζ_{ij} (collisions)
H	37.0	0.3000	—
O	106.7	0.3050	—
OH	79.8	0.3147	—
N_2	71.4	0.3798	4.5
O_2	106.7	0.3467	4.5
H_2	59.7	0.2827	200.0
CO	91.7	0.3690	4.6
CO_2	195.2	0.3941	2.5
H_2O	260.0	0.2800	4.0
HO_2	168.0	0.3068	—
HCO	187.0	0.3465	—
Ar	93.3	0.3542	—

Molecular interactions for the transport property calculations were represented by the Lennard-Jones (12:6) potential, with the use of the force constants given in table 1. Except for σ_H, these are all values recommended by Svehla (1962). The value for σ_H is about 10% higher than Svehla's recommendation. The sensitivity of the computed burning velocities of hydrogen–air flames to the assumed value of σ_H is discussed by Dixon-Lewis (1979).

Most of the remaining data for the transport property calculations have been given by Dixon-Lewis (1968, 1972). Because H_2O is the polar component present in major concentration in all the mixtures studied, and because the theory will deal only with mixtures containing not more than one polar component, all other species were considered to be non-polar.

The collision numbers ζ_{ij} assumed for rotational relaxation of each species i on colliding with any other species j are given in the fourth column of table 1. These collision numbers are only required for those polyatomic molecules included in the thermal conductivity calculation.

(*c*) *Reaction rate coefficients and equilibrium constants*

The expressions used for the forward reaction rate coefficients and the independent equilibrium constants are summarized in table 2. The rate parameters for the reactions that do not involve carbon containing compounds are the mean values derived by Dixon-Lewis (1979) from a study of premixed flames in hydrogen–oxygen–nitrogen mixtures. In reactions (xvi) and (xvii) the chaperon efficiencies of carbon monoxide and carbon dioxide were assumed to be the same as that of nitrogen. In reaction (xv) the chaperon efficiency of carbon monoxide was again assumed to be the same as that of nitrogen, but $k_{15,\mathrm{CO_2}}$ was assigned the expression derived by Walkauskas & Kaufman (1975) from their low temperature studies of hydrogen atom recombination. No high temperature data are available for carbon dioxide as chaperon.

The expressions for k_{21}, k_{22} and k_{23} have been discussed by Baulch *et al.* (1976) and Dixon-Lewis & Williams (1977), with very similar results. The expression for k_{21} recommended by Baulch & Drysdale (1974) has been used. Chaperon efficiencies in reactions (xxii) and (xxiii) are mostly unknown, and, in common with Baldwin *et al.* (1972), it is assumed that all the efficiencies are the same as in reaction (iv). The parameters for both reactions at 773 K, and the chaperon efficiency of carbon monoxide in reaction (iv), are based on a quantitative treatment of the second explosion limits in hydrogen–carbon monoxide–oxygen mixtures at that temperature (Baldwin *et al.* 1972).

PHILOSOPHICAL TRANSACTIONS OF THE ROYAL SOCIETY A MATHEMATICAL, PHYSICAL & ENGINEERING SCIENCES

TABLE 2. PARAMETERS OF EXPRESSIONS FOR FORWARD RATE COEFFICIENTS AND EQUILIBRIUM CONSTANTS USED IN CALCULATION

(Rate coefficients are expressed as $k = AT^B \exp(-C/T)$ and equilibrium constants as $K = DT^E \exp(-F/T) = k_{\text{forward}}/k_{\text{reverse}}$, both in appropriate cm mol s units.)

	reaction	A	B	C/K	D	E	F/K
(i)	$OH+H_2 \rightleftharpoons H_2O+H$	1.17×10^{9}	1.3	1825	0.21	0	−7640
(ii)	$H+O_2 \rightleftharpoons OH+O$	1.42×10^{14}	0	8250	300.0	−0.372	8565
(iii)	$O+H_2 \rightleftharpoons OH+H$	1.8×10^{10}	1.0	4480	2.27	0	938
†(iv)	$H+O_2+H_2 \rightleftharpoons HO_2+H_2$	1.03×10^{18}	−0.72	0	0.745	0	−23380
(vii)	$H+HO_2 \rightleftharpoons OH+OH$	1.4×10^{14}	0	540	—	—	—
(vii *a*)	$H+HO_2 \rightleftharpoons O+H_2O$	1.0×10^{13}	0	540	—	—	—
(xii)	$H+HO_2 \rightleftharpoons H_2+O_2$	1.25×10^{13}	0	0	—	—	—
(xiii)	$OH+HO_2 \rightleftharpoons H_2O+O_2$	7.5×10^{12}	0	0	—	—	—
‡(xiv)	$O+HO_2 \rightleftharpoons OH+O_2$	(*a*) 1.4×10^{13}	0	540	—	—	—
		(*b*) 1.25×10^{12}	0	0	—	—	—
(xv)	$H+H+H_2 \rightleftharpoons H_2+H_2$	9.2×10^{16}	−0.6	0	0.24	0	−52590
	$H+H+N_2 \rightleftharpoons H_2+N_2$	1.0×10^{18}	−1.0	0	—	—	—
	$H+H+Ar \rightleftharpoons H_2+Ar$	1.0×10^{18}	−1.0	0	—	—	—
	$H+H+O_2 \rightleftharpoons H_2+O_2$	1.0×10^{18}	−1.0	0	—	—	—
	$H+H+H_2O \rightleftharpoons H_2+H_2O$	6.0×10^{19}	−1.25	0	—	—	—
	$H+H+CO \rightleftharpoons H_2+CO$	1.0×10^{18}	−1.0	0	—	—	—
	$H+H+CO_2 \rightleftharpoons H_2+CO_2$	5.49×10^{20}	−2.0	0	—	—	—
(xvi)	$H+OH+M \rightleftharpoons H_2O+M$						
	$M = H_2, O_2, N_2, CO, CO_2, Ar$	1.6×10^{22}	−2.0	0	—	—	—
	$M = H_2O$	8.0×10^{22}	−2.0	0	—	—	—
(xvii)	$H+O+M \rightleftharpoons OH+M$						
	$M = H_2, O_2, N_2, CO, CO_2, Ar$	6.2×10^{16}	−0.6	0	—	—	—
	$M = H_2O$	3.1×10^{17}	−0.6	0	—	—	—
(xviii)	$OH+OH \rightleftharpoons O+H_2O$	5.75×10^{12}	0	390	—	—	—
(xxi)	$OH+CO \rightleftharpoons CO_2+H$	1.5×10^{7}	1.3	−385	3.83×10^{-7}	1.19	−13067
†(xxii)	$O+CO+H_2 \rightleftharpoons CO_2+H_2$	5.4×10^{15}	0	2300	—	—	—
†(xxiii)	$H+CO+H_2 \rightleftharpoons HCO+H_2$	5.0×10^{14}	0	755	1.7	0	−7080
					(0.095	0.331	−14430)§
(xxiv)	$HCO+O_2 \rightleftharpoons HO_2+CO$						
(xxv)	$H+HCO \rightleftharpoons H_2+CO$						
(xxvi)	$OH+HCO \rightleftharpoons H_2O+CO$	see text					
(xxvii)	$O+HCO \rightleftharpoons OH+CO$						

† Chaperon efficiencies relative to $H_2 = 1.0$ are 0.44, 0.35, 6.5, 0.74, 1.47 and 0.35 for N_2, O_2, H_2O, CO, CO_2 and Ar respectively (Dixon-Lewis & Williams 1977; Boularas *et al.* 1981).

‡ $k_{14} = k_{14a} + k_{14b}$.

§ The heat of dissociation of HCO has until recently been a matter of controversy, with values of approximately 67 and 126 kJ mol^{-1} being canvassed. Recent work by Fletcher & Pilcher (1970), quoted by Baulch *et al.* (1976), favours the lower value as given by JANAF (1974); and the unparenthesized expression for the equilibrium constant K_{23} is based on this. The expression in parentheses is based on the higher value. These expressions are to be discussed in §3 along with the rate coefficients for reactions (xxiv) to (xxvii).

In the interpretation of the hydrogen–carbon monoxide–oxygen second limits, Baldwin *et al.* (1972) assumed that all HCO formation is followed by reaction (xxiv). As a result no information is available about k_{24}, k_{25}, k_{26} or k_{27} from this source. As indicated in table 2, there has also until recently been some controversy about the heat of formation of the formyl radical, and hence about the relation between the forward and reverse rate coefficients of reaction (xxiii). It is more particularly towards these reactions that attention will be directed in the present paper.

One flame containing argon as diluent instead of nitrogen was also studied. The chaperon efficiency of argon in reaction (xv) has been discussed by Dixon-Lewis (1979), and its efficiency in reaction (iv) has recently been deduced by Boularas *et al.* (1981) from measurements of the burning velocities of a series of low temperature, fuel-rich hydrogen–oxygen–argon flames. In reactions (xvi) and (xvii) the efficiencies of argon were assumed to be the same as those of nitrogen.

Equilibrium constants and other thermodynamic data are based on JANAF (1971). The expressions for K_{15}, K_{16}, K_{17} and K_{21} were deduced by simple parametric fitting of the van't Hoff isochore to equilibrium constants at 1500 and 2500 K from the tabulation. The expressions for K_1, K_2 and K_3 are those due to Del Greco & Kaufman (1963).

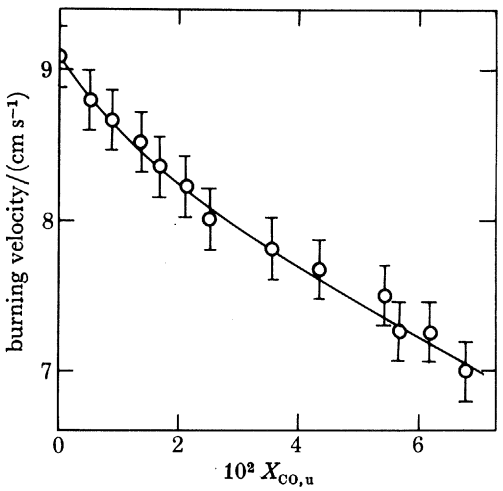

FIGURE 1. Burning velocities of flames having initial mole fraction compositions: $X_{H_2,u} = 0.1685$, $X_{N_2+CO,u} = 0.7855$ and $X_{O_2,u} = 0.0460$ at a pressure of 1 atm, with $T_u = 336$ K. Burning velocities are referred to unburned gas at 291 K and 101 kPa.

3. RESULTS

(*a*) *Addition of small amounts of carbon monoxide to a low temperature, fuel-rich hydrogen–oxygen–nitrogen flame*

A number of flames at atmospheric pressure having the initial mole fraction composition $X_{H_2,u} = 0.1685$, $X_{N_2+CO,u} = 0.7855$ and $X_{O_2,u} = 0.0460$, with $T_u = 336$ K, and with the $N_2 + CO$ mixture containing between 0 and 10% carbon monoxide, were supported on an Egerton–Powling type of flat flame burner. Burning velocities were measured by the powder particle tracking technique as described by Dixon-Lewis & Isles (1969). The resulting burning velocities are shown in figure 1. The effect of the carbon monoxide is to cause a small decrease in the burning velocity.

The flame having $X_{H_2,u} = 0.1685$, $X_{N_2,u} = 0.7237$, $X_{CO,u} = 0.0618$ and $X_{O_2,u} = 0.0460$, with $T_u = 336$ K and a measured burning velocity of 7.2 ± 0.2 cm s^{-1} referred to gases at 291 K and 101 kPa was selected for theoretical investigation. Burning velocities for this flame were initially calculated on the assumptions that, in addition to the hydrogen–oxygen–nitrogen flame reactions, the flame receives a contribution from the carbon monoxide due, first, to reaction (xxi) alone and, secondly, to reactions (xxi) and (xxii) together. The predicted burning velocities were 10.2 and 10.0 cm s^{-1}, quoted on the same basis as above. Clearly then, some new chain termination mechanism must operate in the flame, and this must be associated

TABLE 3. COMPUTED BURNING VELOCITIES OF FLAMES HAVING INITIAL COMPOSITION $X_{H_2,u} = 0.1685$, $X_{N_2,u} = 0.7237$, $X_{CO,u} = 0.0618$ AND $X_{O_2,u} = 0.0460$, WITH $T_u = 336$ K, ON SEVERAL ASSUMPTIONS ABOUT MAGNITUDES OF K_{23}, k_{24} AND k_{25}, EXPRESSED IN cm mol s UNITS

(Computed burning velocities referred to gas at 291 K and 101 kPa. Remaining reaction rate parameters from table 2.)

set	K_{23}	k_{24}	k_{25}	$S_{u,calc}/(cm\ s^{-1})$
1	$0.095\ T^{0.331} \exp(+14430/T)$	3×10^{13}	0	7.2
			3×10^{12}	6.4
			6×10^{12}	6.3
			1.5×10^{13}	6.25
		3×10^{12}	0	7.5
			3×10^{11}	6.9
			1×10^{12}	6.5
2	$1.7 \exp(+7080/T)$	3×10^{13}	0	8.59
			6×10^{13}	7.03 (2A)
		3×10^{12}	6×10^{12}	8.92
			4×10^{13}	7.08 (2B)
			6×10^{13}	6.52
		3×10^{11}	3.2×10^{13}	7.16 (2C)
		0	4×10^{13}	6.77
			3×10^{13}	7.17

with the reactions of the formyl radical. It is interesting to note that the effect of reaction (xxi) alone is actually to increase the burning velocity above that for the hydrogen–oxygen–nitrogen flame without carbon monoxide, for which both the predicted and measured burning velocities are 9.1 cm s^{-1}. The reason for the increase in the prediction for the carbon monoxide containing flame is to be found in a small increase in the final flame temperature, caused by the numerically higher enthalpy change in reaction (xxi) compared with the analogous reaction (i).

The next stage is the investigation of the reactions of the formyl radical. In the particular flame studied, the concentrations of OH and O are very much smaller than the concentration of hydrogen atoms, so that reactions (xxvi) and (xxvii) are relatively unimportant. This leaves reactions (−xxiii), (xxiv) and (xxv) competing for the formyl radical. On the assumptions that reactions (xxiv) and (xxv) both have zero activation energy, the results of several calculations on this basis are given in table 3. In set 1 of calculations the equilibrium constant K_{23} was assigned the expression $K_{23} = 0.095\ T^{0.331} \exp(+14430/T)$ cm^3 mol^{-1} (see table 2). To satisfy the measured burning velocity of 7.2 cm s^{-1} it was found necessary, for reasonable values of k_{24}, to have $k_{25} < k_{24}$. This result is contrary to the findings of Mack & Thrush (1973) and Washida *et al.* (1974), who obtained $k_{25}/k_{27} = 4 \pm 1$ and $k_{24}/k_{27} = (2.74 \pm 0.2) \times 10^{-2}$ respectively at 300 K. The results given as set 2, with $K_{23} = 1.7 \exp(+7080/T)$ cm^3 mol^{-1}, appear much more plausible in this respect. Although the low value of the ratio k_{24}/k_{27} has not been confirmed, so that the evidence is not absolutely compelling, the analysis nevertheless strongly favours the smaller enthalpy change for reaction (xxiii).

The results given in set 2 of table 3 lead to an estimate of $k_{25} = (4 \pm 1) \times 10^{13}$ cm^3 mol^{-1} s^{-1}. In the following sections of the paper combinations of $k_{25} = 4 \times 10^{13}$ with $k_{24} = 3 \times 10^{12}$ (set 2B), and occasionally $k_{25} = 6 \times 10^{13}$ with $k_{24} = 3 \times 10^{13}$ (set 2A) or $k_{25} = 3.2 \times 10^{13}$ with $k_{24} = 3 \times 10^{11}$ (set 2C), will be adopted. Set 2C gives a ratio k_{25}/k_{24} close to that which would

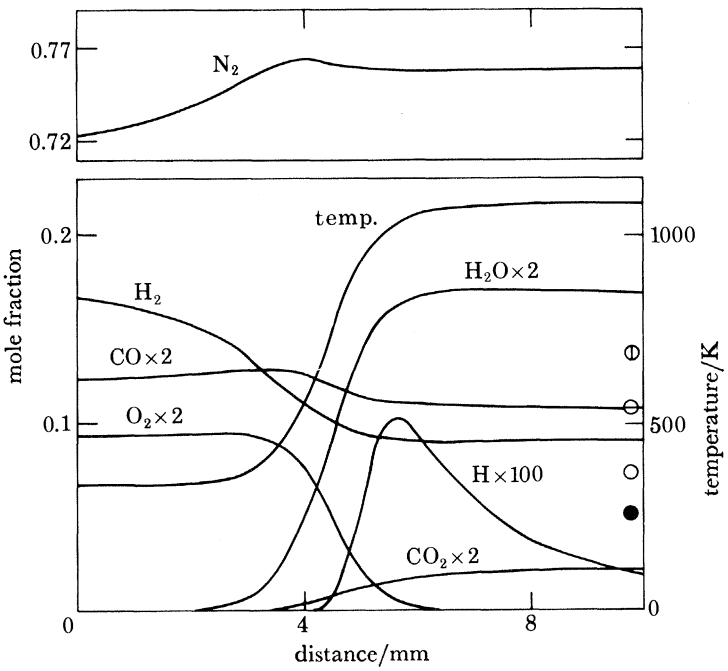

FIGURE 2. Computed temperature profile and mole fraction profiles for stable species and hydrogen atoms in a flame having initial mole fraction composition: $X_{H_2,u} = 0.1685$, $X_{N_2,u} = 0.7237$, $X_{CO,u} = 0.0618$ and $X_{O_2,u} = 0.0460$ at a pressure of 1 atm, with $T_u = 336$ K. Transport parameters are from table 1. Reaction rate parameters are from table 2 and set 2B, table 3. Computed burning velocity, $S_{u,calc} = 7.08$ cm s^{-1}, referred to unburned gas at 291 K and 101 kPa. Points towards right of figure indicate mole fractions in equilibrium products at 1080 K: ⊖, H_2; ○, $CO\times2$; ⊕, $H_2O\times2$; ●, $CO_2\times2$.

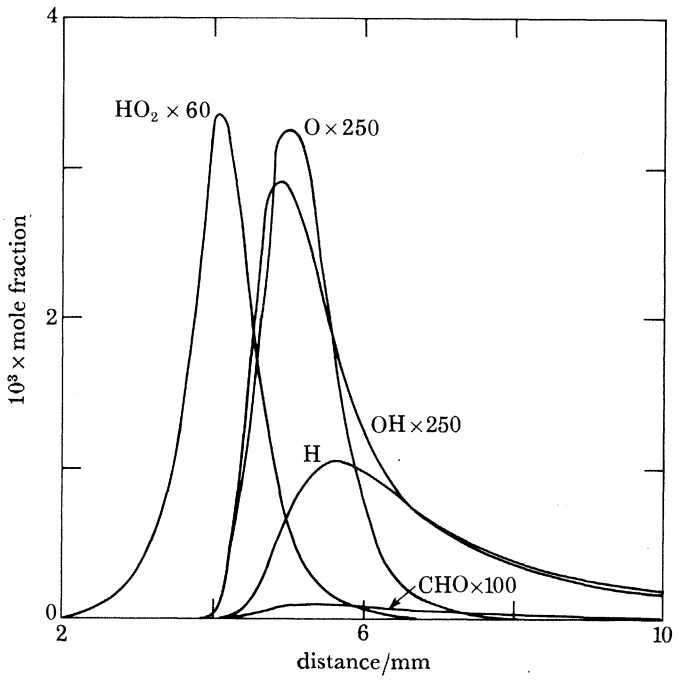

FIGURE 3. Computed mole fraction profiles for radical species in a flame having initial mole fraction composition: $X_{H_2,u} = 0.1685$, $X_{N_2,u} = 0.7237$, $X_{CO,u} = 0.0618$ and $X_{O_2,u} = 0.0460$ at a pressure of 1 atm, with $T_u = 336$ K. Transport parameters are from table 1. Reaction rate parameters are from table 2 and set 2B, table 3. Distances are from the same reference zero as in figure 2.

PHILOSOPHICAL TRANSACTIONS OF THE ROYAL SOCIETY A MATHEMATICAL, PHYSICAL & ENGINEERING SCIENCES

be obtained by combining k_{25}/k_{27} from Mack & Thrush (1973) with k_{24}/k_{27} from Washida *et al.* (1974).

For $k_{25} = 4 \times 10^{13}$ and $k_{24} = 3 \times 10^{12}$ (set 2B), and with the remaining reaction rate parameters as in table 2, the temperature profile and mole fraction profiles for the stable species and the hydrogen atom in the flame of table 3 are shown in figure 2. Figure 3 shows the corresponding radical mole fraction profiles. The ratio X_{CO}/X_{CO_2} in the burnt gas region of the flame (10 mm after the position of maximum hydrogen atom concentration) was calculated to be 4.3, compared with $X_{H_2}/X_{H_2O} = 1.08$. For equilibration of the water gas reaction a ratio $X_{CO}X_{H_2O}/X_{CO_2}X_{H_2} = 0.9$ would be expected at 1080 K, and this would entail mole fractions of H_2, CO, H_2O and CO_2 given by the points shown at the right of figure 2. Clearly the water gas equilibrium is not achieved. On the other hand, reaction (i) is more or less equilibrated in the burnt gas region of the flame, as is shown in figure 3 by the constant ratio $X_H/X_{OH} \approx 250$. The lack of equilibration is therefore associated in particular with reaction (xxi).

(*b*) *Addition of a trace of carbon dioxide to gases entering a low temperature hydrogen–oxygen–nitrogen flame*

Dixon-Lewis *et al.* (1965) examined reaction (xxi) by mass spectrometric measurement of the ratio X_{CO_2}/X_{N_2} at a number of distances through a flame at atmospheric pressure having the initial composition $X_{H_2,u} = 0.1883$, $X_{N_2,u} = 0.7594$, $X_{O_2,u} = 0.0462$ and $X_{CO_2,u} = 0.0061(5)$, with $T_u = 336$ K. These measurements are shown as the points in figure 4. The results were analysed by Dixon-Lewis (1972) by means of a flame structure calculation; and he later (Dixon-Lewis 1979) used the conclusions from this analysis, in conjunction with the mean expression $k_{21} = 1.5 \times 10^7\, T^{1.3} \exp(+385/T)$ cm^3 mol^{-1} s^{-1} recommended by Baulch & Drysdale (1974), to calibrate the hydrogen atom concentrations in the flame. If the mean recommended value of k_{21} is used in the present calculation together with the other rate parameters from table 2, the overall model leads to the computed ratios X_{CO_2}/X_{N_2} shown by the lower line in figure 4. The upper line was obtained when k_{21} was reduced by 10 % below the mean expression. Agreement with experiment is satisfactory in both cases, and shows the flame model to be consistent with the calibration value of k_{21} when the additive is carbon dioxide, and reaction (xxi) proceeds in the reverse direction.

(*c*) *Addition of carbon monoxide to a low temperature hydrogen–oxygen–argon flame*

As a further check on the validity of the parameters associated with the ratio k_1/k_{21}, the mole fraction ratio X_{CO}/X_{CO_2} was measured in the burnt gas above a hydrogen–carbon monoxide–oxygen–argon flame at atmospheric pressure having the initial mole fraction composition $X_{H_2,u} = 0.1560$, $X_{CO,u} = 0.0610$, $X_{Ar,u} = 0.7487$ and $X_{O_2,u} = 0.0343$, with $T_u = 350$ K. Mass spectrometric measurement gave $X_{CO,b}/X_{CO_2,b} = 6.4$. Computation of the complete properties of the flame led to $X_{CO,b}/X_{CO_2,b} = 6.33$, in good agreement with the measured value. At the same time the computed ratio $X_{H_2,b}/X_{H_2O,b} = 1.59$ at $T_b = 1095$ K. Achievement of the water gas equilibrium at this temperature would demand a value of 0.93 for the ratio $X_{CO}X_{H_2O}/X_{CO_2}X_{H_2}$, so that clearly the measured ratio is largely rate determined.

PHILOSOPHICAL TRANSACTIONS OF THE ROYAL SOCIETY A MATHEMATICAL, PHYSICAL & ENGINEERING SCIENCES

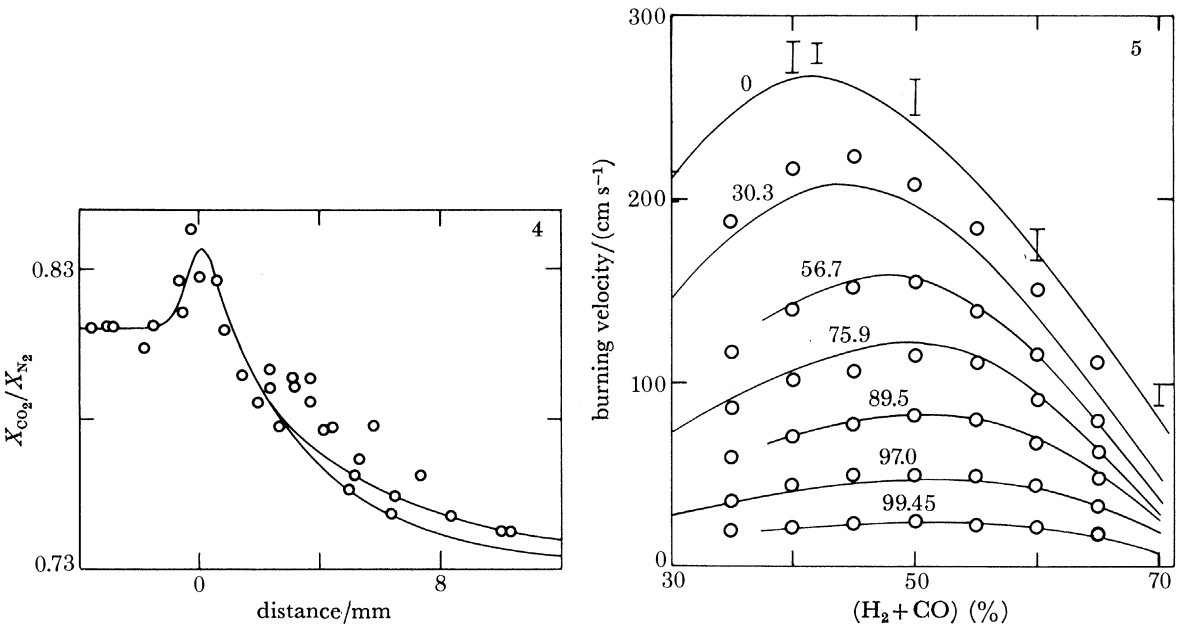

FIGURE 4. Disappearance of carbon dioxide in flame having initial mole fraction composition $X_{H_2,u} = 0.1883$, $X_{N_2,u} = 0.7594$, $X_{O_2,u} = 0.0462$ and $X_{CO_2,u} = 0.0061(5)$ at atmospheric pressure, with $T_u = 336$ K, showing comparison between computed lines and experimental points. Transport parameters for computation are from table 1. Lower line, reaction rate parameters from table 2; upper line, rate parameters also from table 2, but with $k_{21} = 1.35 \times 10^7\ T^{1.3} \exp(+385/T)$ cm^3 mol^{-1} s^{-1}. Computed burning velocity $S_{u,calc} = 9.2$ cm s^{-1}, quoted for unburned gases at 291 K and 101 kPa.

FIGURE 5. Burning velocities of dry hydrogen–carbon monoxide–air mixtures at atmospheric pressure, with $T_u = 298$ K, comparing computed lines with points representing observations of Scholte & Vaags (1959*c*). Number above each curve gives percentage of carbon monoxide in the H_2+CO fuel. Transport parameters for computation are from table 1. Reaction rate parameters are as in set F, table 4.

(*d*) *Burning velocities of hydrogen–carbon monoxide–air flames at atmospheric pressure*

It is well known that the oxidation of carbon monoxide is very sensitive to the presence of traces of hydrogen, water vapour or other hydrogen-containing compounds; and that the burning velocities of carbon monoxide–air mixtures increase sharply on addition of small quantities of such compounds. Burning velocities of carbon monoxide–air mixtures containing only a little added hydrogen or water vapour will be considered more particularly in §3(*e*). The present section is concerned with the complete range of hydrogen–carbon monoxide mixtures as fuels, mixtures containing 0.55, 3.0, 10.5, 24.1, 43.3, 69.7 and 100% hydrogen being used. Burning velocities of mixtures containing between 35 and 65% of these fuels in air at atmospheric pressure have been measured by Scholte & Vaags (1959*c*). For the studies with the fuels containing 0.55 and 3.0% hydrogen, the gases and air were dried with concentrated sulphuric acid to avoid acceleration of the flame by moisture. The effect of small amounts of water vapour on the burning velocities of the other mixtures was found to be negligible.

The flames studied by Scholte & Vaags (1959*c*) were supported as straight-sided cones on a constant velocity profile nozzle, and the linear unburnt gas velocities V were calculated by dividing the area of the burner port into the total volumetric gas flow. The burning velocities were then derived by measuring the cone half-angles, α, and using $S_u = V \sin \alpha$. Because of

TABLE 4. COMPARISON OF PREDICTED BURNING VELOCITIES OF SEVERAL HYDROGEN–CARBON MONOXIDE–AIR FLAMES WITH MEASUREMENTS OF SCHOLTE & VAAGS (1959*c*), TO DEMONSTRATE OVERALL EFFECTS OF REACTIONS (xxii) AND (xxiii)

(In all cases $T_u = 298$ K and $p = 1$ atm.)

flame	composition of fuel $X_{H_2,u}$	composition of fuel $X_{CO,u}$	$S_{u,obs}$ / (cm s^{-1})	$S_{u,calc}$ / (cm s^{-1}) set D†	set E‡	set F§
	(*a*) Flames containing 60 % fuel + 40 % air, by volume, in unburnt gas					
A	1.0000	0	175	170	170	170
B	0.6970	0.3030	151	148.4	148.0	136.7
C	0.2410	0.7590	90	113.9	112.2	94.6
D	0.1050	0.8950	68	87.9	84.6	73.3
E	0.0300	0.9700	45	—	—	44.7
F	0.0055	0.9945	21	22.7	20.6	19.5
	(*b*) Flames containing 40 % fuel + 60 % air, by volume, in unburnt gas					
G	1.0000	0	275	265	265	265
H	0.6970	0.3030	217	203	202	203
I	0.2410	0.7590	101	109.0	108.3	108.0
J	0.1050	0.8950	71	72.0	71.1	69.2
K	0.0300	0.9700	44	—	—	40.6
L	0.0055	0.9945	21	19.0	20.0	19.6

† Set D: k_{21} as in table 2; $k_{22} = k_{23} = 0$.
‡ Set E: k_{21} and k_{22} as in table 2; $k_{23} = 0$.
§ Set F: k_{21}, k_{22} and k_{23} as in table 2; k_{24} and k_{25} as in set 2B, table 3; $k_{26} = 4 \times 10^{13}$, $k_{27} = 1 \times 10^{13}$ cm^3 mol^{-1} s^{-1}.

small boundary layer effects at the edge of the nozzle, this approach to calculating the gas velocity introduces a certain amount of averaging into the experiment, and the precision would have been improved if these velocities had been directly measured. However, Dixon-Lewis (1979) has shown that when such measurements are made for the unburnt gas approaching a flame, flow divergence in the flame zone itself necessitates a correction to the measured velocity to take account of such divergence up to a reference plane at the hot side of the flame. When such corrections were applied to several hydrogen–air burning velocities precisely measured as above by Edmondson & Heap (1971) and Günther & Janisch (1971), they led to results in reasonable agreement with theoretical predictions, and with the results of Jahn (1934) and Scholte & Vaags (1959*a*) for those flames. There is reason therefore to suppose that the results of Scholte & Vaags (1959*c*) for hydrogen–carbon monoxide–air mixtures are adequate for the present purpose. Their results for these mixtures are shown as the points in figure 5.

For this set of flames, predictions will first be considered for two series of mixtures of fuel with air, containing respectively 60 % and 40 % fuel. The fuels were hydrogen–carbon monoxide mixtures containing 100 %, 69.7 %, 24.1 %, 10.5 % and 0.55 % hydrogen respectively. Calculations were again performed under three sets of assumptions:

(i) that the carbon monoxide contributes to the flame mechanism by way of reaction (xxi) alone (set D);

(ii) that it contributes by way of a combination only of reactions (xxi) and (xxii) (set E); and

(iii) that the whole series of reactions (xxi) to (xxvii) becomes involved (set F).

Reaction rate parameters were taken as necessary from tables 2 and 3 (set 2B).

The predicted burning velocities of the several flames, on each of these assumptions, are compared in table 4 with the measurements of Scholte & Vaags (1959*c*). Inspection of table 4 shows that, certainly for the mixtures containing only small amounts of carbon monoxide, the bulk of the effect of replacing hydrogen by carbon monoxide may be explained without involving any of the reactions (xxii) to (xxvii). Further, in no situation does reaction (xxii) exert more than a minor influence on the burning velocity, at least when k_{22} is assigned the independently obtained expression given in table 2.

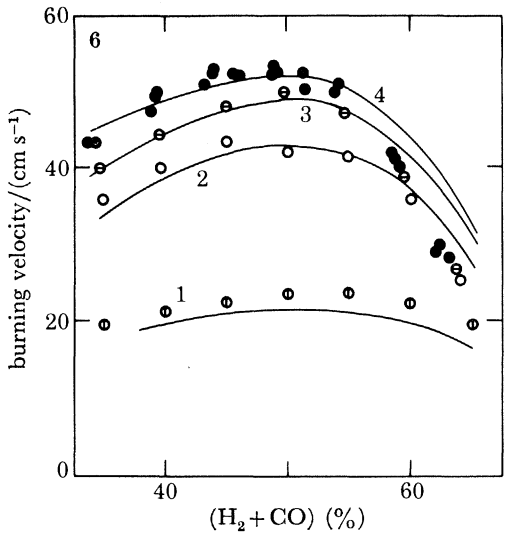

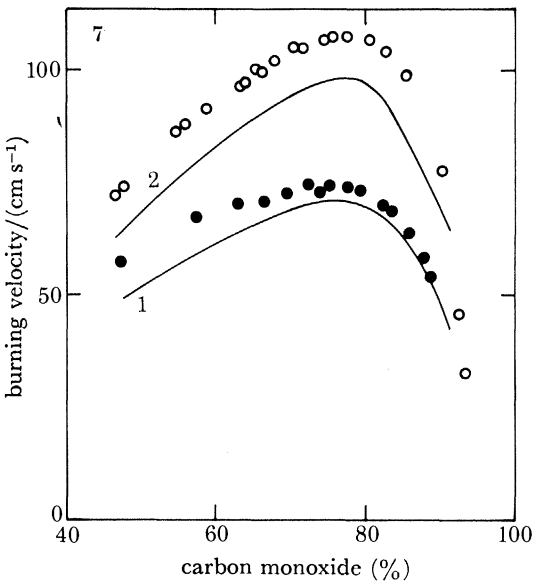

FIGURE 6. Effect of addition of water vapour on burning velocities of flames of 0.55% hydrogen + 99.45% carbon monoxide in air at atmospheric pressure, with T_u = 298 K, comparing computed lines with points representing observations of Scholte & Vaags (1959*b*). Curve 1 and ⊕, no added water; curve 2 and ○, 1.20% added water; curve 3 and ⊖, 1.87% added water; curve 4 and ●, 2.30% added water. Water additions are percentages of the total mixture, and were regarded in computations as replacing nitrogen. Transport parameters for computations are from table 1. Reaction rate parameters are as in set F, table 4.

FIGURE 7. Burning velocities of carbon monoxide–oxygen flames containing traces of added hydrogen and water vapour at atmospheric pressure, with T_u = 298 K, comparing computed lines with points representing observations of Jahn (1934). Curve 1, carbon monoxide contained 1.35% H_2O; curve 2, carbon monoxide contained 1.35% H_2O + 1.5% H_2. In both cases oxygen contained 1.5% N_2. Transport parameters for computations are from table 1. Reaction rate parameters are as in set F, table 4.

For the compositions studied, table 4 also shows that set F of rate parameters, based on tables 2 and 3, predicts burning velocities in reasonable agreement with the experiments of Scholte & Vaags (1959*c*). A more extended comparison is shown in figure 5, in which the lines show the burning velocities computed with the parameters of set F. Over the composition ranges for which the lines are drawn, the calculations were normally performed at 5% intervals in the fuel content of the combustible mixture. Agreement with the experimental points is satisfactory over the whole composition range.

The set F of rate parameters in table 4 was further examined in relation to the effect of replacing the pair 2B of rate coefficients k_{24} and k_{25} in table 3 by the pairs 2A and 2C. For the fuel containing 10.5% hydrogen, the predicted burning velocities of the 60% fuel + 40% air flame were 74.6, 73.3 and 71.5 cm s^{-1} for pairs 2A, 2B and 2C, compared with a measured

68 cm s^{-1}. For the similar 40 % fuel + 60 % air flame the corresponding predictions were 69.8, 69.2 and 68.7, compared with a measured 71 cm s^{-1}. These differences are not sufficiently large to allow a distinction to be made between the three pairs on the basis of the measured burning velocity. The concentrations of hydroxyl radicals and oxygen atoms in the 60 % fuel flame are also too small for effects of reactions (xxvi) and (xxvii) to be significant. In the 40 % fuel + 60 % air flame, table 4 shows that the overall effect of the series of reactions involving the formyl radical is also small. Hence no reliable information about k_{26} or k_{27} is available from this source either. These rate coefficients are estimated to be of the same order as, and slightly less than, k_{25}.

(*e*) *Flames in carbon monoxide–air mixtures containing traces of hydrogen or water vapour, or both*

Burning velocities of carbon monoxide–air mixtures containing traces of hydrogen or water vapour, or both, have been measured by Jahn (1934), Badami & Egerton (1955) and Scholte & Vaags (1959*b*). Jahn (1934) has also measured the burning velocities of a series of carbon monoxide–oxygen mixtures sensitized in the same way; and Wires *et al.* (1959) have used the early, constant pressure stages of flame travel after central ignition in a constant volume bomb to measure flame velocities in $2CO + O_2$ mixtures containing some hydrogen or deuterium. Each of these investigations will now be considered in turn, and predictions from the flame model will be compared with the results. Reaction rate parameters in all cases are taken from tables 2 and 3, with the use of the same combination as in set F of table 4.

(i) For a fuel consisting of 0.55 % hydrogen and 99.45 % carbon monoxide, Scholte & Vaags (1959*b*) examined the effect of additions of 1.20, 1.87 and 2.30 % water vapour on the burning velocities of fuel–air mixtures containing between 35 % and 65 % fuel. The water concentrations were expressed as percentages of the total mixture. Their results are shown as the points in figure 6. The lines in the figure show the burning velocities predicted from the flame model.

(ii) Jahn (1934) measured the burning velocities of a range of carbon monoxide–air mixtures at atmospheric pressure, in which the carbon monoxide contained, in one series of experiments, 1.5 % hydrogen *and* 1.35 % water vapour, and in a second series, 1.35 % water vapour only. The measured burning velocities of the 50 % fuel + 50 % air mixtures in the two series were 45.6 and 32.9 cm s^{-1} respectively. The corresponding predictions from the flame model were 44.9 and 29.8 cm s^{-1}.

(iii) In two further series of experiments, Jahn (1934) also examined the burning velocities of mixtures of the two samples of carbon monoxide with molecular oxygen containing 1.5 % nitrogen. These measurements are shown as the points, and the predicted burning velocity curves by the lines, in figure 7.

(iv) Badami & Egerton (1955) have used the flame area method to measure the burning velocities of several series of carbon monoxide–air mixtures containing traces of hydrogen and water vapour, with compositions near the lean flammability limits. The points showing their results are compared with the predicted burning velocity curves in figures 8 and 9.

(v) The burning velocities of dry, stoichiometric mixtures of carbon monoxide and oxygen, containing also traces of hydrogen, were measured at a pressure of 1 atm† by Wires *et al.* (1959). The burning velocities predicted for four of their flames by the present model are compared with their results in table 5.

† 1 atm ≈ 101 kPa.

PHILOSOPHICAL TRANSACTIONS OF THE ROYAL SOCIETY A MATHEMATICAL, PHYSICAL & ENGINEERING SCIENCES

The quantitative predictions of the model are in fair agreement with four of the sets of measurements, particularly when the difficulty of introducing precisely measured traces of water vapour into the gas mixtures is borne in mind. In the fifth set of measurements, those of Badami & Egerton (1955), the discrepancy may well be due to experimental problems of definition of the diameters of the circular flat flames, due to diffuseness at their edges. This could introduce considerable uncertainty into the flame areas. More recent measurements of flat flame burning velocities have used powder particle tracking techniques to measure the velocity of approach of the gas to the flame, but these techniques have not been applied to the carbon monoxide–air flames near the lean limit.

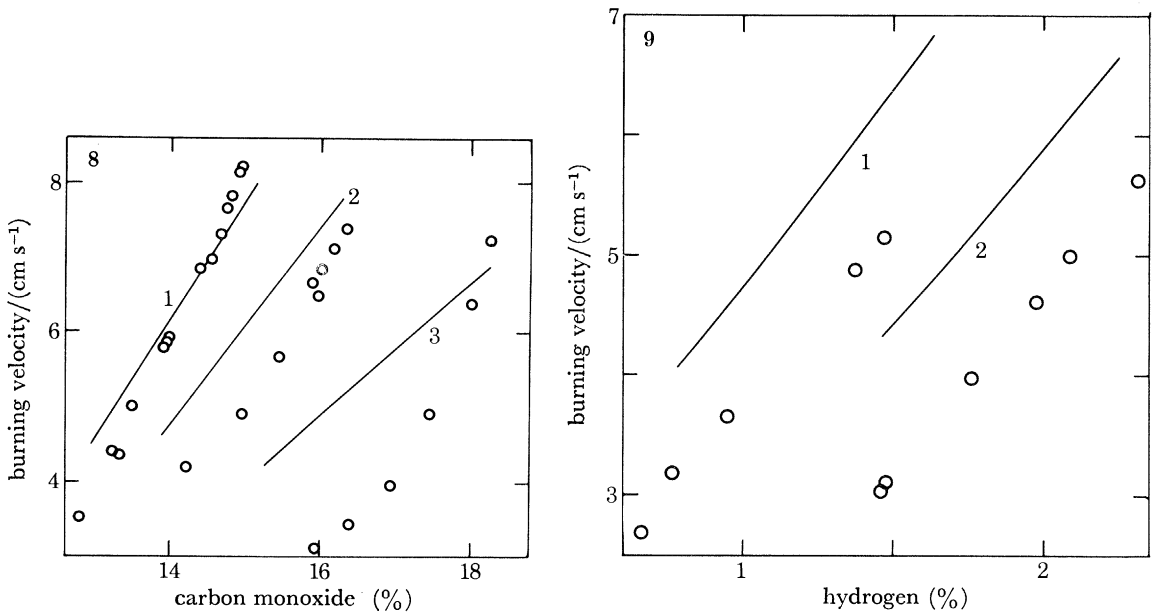

FIGURE 8. Burning velocities of carbon monoxide–air flames containing traces of water vapour at atmospheric pressure, comparing computed lines with points representing observations of Badami & Egerton (1955). Burning velocities are quoted on the basis of unburned gas at 291 K and 101 kPa. Curve 1, 1.35% H_2O in mixture; curve 2, 0.5% H_2O; curve 3, 0.12% H_2O. Following experimental procedure of Badami & Egerton, lines were computed for $T_u = 453$ K, after which a preheat correction was applied to initial mixture compositions to give the same final temperature from an assumed initial temperature of 291 K. Mixtures at 453 K thus contain 1.685% less carbon monoxide than plotted. Transport parameters for computation are from table 1. Reaction rate parameters are as in set F, table 4.

FIGURE 9. Burning velocities of carbon monoxide–air mixtures containing traces of water vapour and hydrogen at atmospheric pressure, comparing computed lines with points representing observations of Badami & Egerton (1955). Burning velocities are quoted on the basis of unburned gas at 291 K and 101 kPa. All mixtures contained 0.12% water vapour. Curve 1, 11.65% CO in mixture; curve 2, 10.57% CO, both on the assumption of $T_u = 291$ K and after application of preheat correction to composition as in figure 8. Actual flame compositions, with $T_u = 453$ K, contained 1.685% less carbon monoxide than quoted. Transport parameters for computations are from table 1. Reaction rate parameters are as in set F, table 4.

(*f*) *Structures of two hydrogen–carbon monoxide–oxygen flames at reduced pressure*

(i) Fenimore & Jones (1959) measured the temperature profile and the composition profiles for the stable species in a burner-stabilized flame at 5.32 kPa (40 Torr) pressure having a supply stream of mole fraction composition $X_{H_2} = 0.276$, $X_{CO} = 0.058$, $X_{O_2} = 0.127$ and $X_{Ar} = 0.539$. The measured linear velocity of fresh gas at the burner was 59.7 cm s^{-1}, quoted on the basis of gas at 298 K and 5.32 kPa. The points in figure 10 show the measured temperatures and

TABLE 5. COMPARISON OF PREDICTED BURNING VELOCITIES OF STOICHIOMETRIC CARBON MONOXIDE–OXYGEN MIXTURES CONTAINING TRACES OF HYDROGEN WITH MEASUREMENTS OF WIRES *et al.* (1959)

(In all cases $T_u = 298$ K and $p = 1$ atm.)

hydrogen (%)	$S_{u,obs}/(\text{cm s}^{-1})$	$S_{u,calc}/(\text{cm s}^{-1})$
0.100	33.7	29.8
0.500	54.3	52.2
2.000	91.3	85.1

the mole fraction ratios X_{H_2}/X_{Ar}, X_{CO}/X_{Ar}, X_{O_2}/X_{Ar}, $X_{H_2O}/2X_{Ar}$ and $2X_{CO_2}/X_{Ar}$, plotted against distance from the burner. Temperatures were measured by means of a fine quartz-coated thermocouple, and compositions by sampling and mass spectrometric analysis. It should be noted, however, that the temperature and composition of the mixture actually *at* the burner surface are not known precisely. On the assumption of zero reaction before this surface is reached, the only defined values at the cold boundary surface of the flame are the overall mass fluxes of the several chemical species present. To solve the computational problem it is necessary to choose a reasonable temperature for the upper surface of the water-cooled porous plate (350 K was chosen in the present instance), and then to allow the concentrations and concentration gradients there to adjust themselves in such a way that the prescribed hot and cold boundary conditions are satisfied when the overall fluxes at the cold boundary take their defined values. The computational procedure is somewhat lengthier than that for a free flame. To optimize the matching with experiment, it may then be necessary (following the computation) slightly to move the distance scale of either the measured or computed results, to compensate for possible error in the assumed cold boundary temperature.

The lines in figure 10 show the computed profiles of the temperature and the mole fraction ratios for the stable species in the flame studied experimentally by Fenimore & Jones (1959). The agreement with experiment is reasonable. Figure 11 shows the computed mole fraction profiles for the radical species in the flame.

(ii) Vandooren *et al.* (1975) measured the temperature and mole fraction profiles in a burner-stabilized flame, again at 5.32 kPa (40 Torr) pressure, having a supply stream of mole fraction composition $X_{H_2} = 0.114$, $X_{CO} = 0.094$ and $X_{O_2} = 0.792$. The measured linear fresh gas velocity at the burner was 63.7 cm s^{-1}, quoted on the basis of gas at 298 K and 5.32 kPa. The points in figure 12 show the measured temperatures and the mole fractions of the stable species, again plotted against distance from the burner. The points in figure 13 similarly show the mole fractions of radicals. All the mole fractions were measured by molecular beam sampling and mass spectrometry. Temperatures were measured with the aid of a ceramic coated Pt/Pt-10 % Rh thermocouple. Again, unfortunately, neither the temperature of the burner surface nor the rate of heat abstraction is quoted. Computation was therefore made exactly as described in §3(*f*) (i).

The profiles resulting from the computations are shown as the lines in figures 12 and 13. Except for water vapour, for which the discrepancy between the predicted and measured profiles may be due to a calibration error, the agreement with experiment for the stable species is very good. Further, the predicted maximum rates of formation of carbon dioxide and water are 1.3×10^{-5} and 3.1×10^{-5} mol cm^{-3} s^{-1} respectively. Both predictions compare extremely well with the maximum rates of 1.3×10^{-5} and 3.2×10^{-5} mol cm^{-3} s^{-1} deduced

PHILOSOPHICAL TRANSACTIONS OF THE ROYAL SOCIETY A MATHEMATICAL, PHYSICAL & ENGINEERING SCIENCES

directly by Vandooren *et al.* (1975) from the experimental observations. There is, however, a large discrepancy between the predicted and measured temperature profiles. In contrast with the measurements, the computations predict that a temperature of 1800 K will not be reached until a distance of some 9–10 cm from the burner. The difference may be due to some catalytic effect at the surface of the thermocouple used for the measurements.

With regard to the radical profiles, there is again some discrepancy between theory and

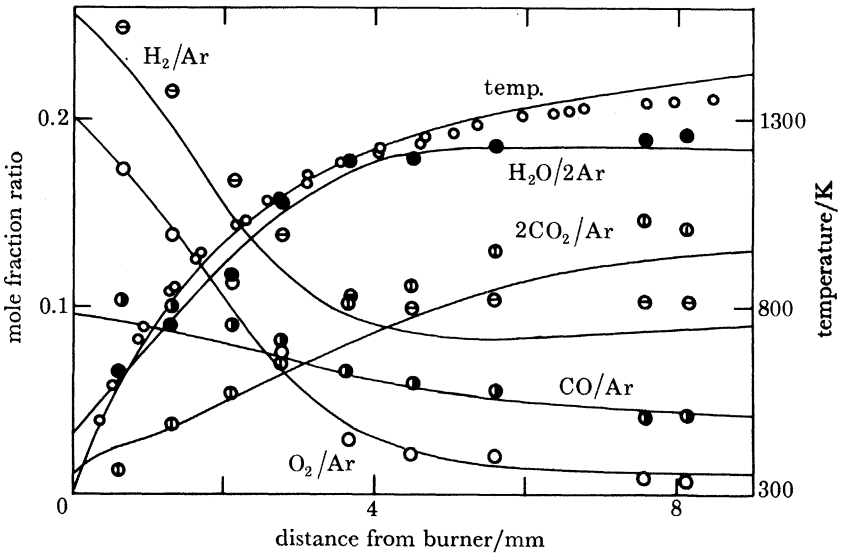

FIGURE 10. Profiles of temperature and mole fraction ratios of stable species against distance from burner in a hydrogen–carbon monoxide–oxygen–argon flame, comparing computed lines with points representing observations of Fenimore & Jones (1959). Mole fraction composition of supply mixture was: $X_{H_2} = 0.276$, $X_{CO} = 0.058$, $X_{O_2} = 0.127$ and $X_{Ar} = 0.539$, with $p = 5.32$ kPa (40 Torr). Flow velocity of fresh gases was 59.7 cm s^{-1}, measured for gas at 298 K and 5.32 kPa. Transport parameters for computation are from table 1. Reaction rate parameters are as in set F ,table 4. Points: ○, temperature; ○, O_2/Ar; ◑, CO/Ar; ⊖, H_2/Ar; ⊙, $2CO_2$/Ar; ●, H_2O/2Ar.

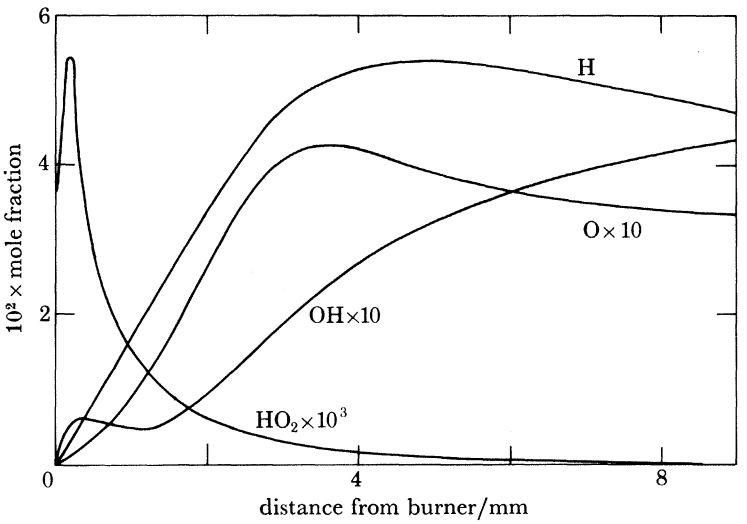

FIGURE 11. Computed profiles of mole fractions of radicals against distance from burner in flame of figure 10. Transport parameters for computations are from table 1. Reaction rate parameters are as in set F, table 4.

experiment, which we believe to be too great to be accounted for by imprecisions in the rate parameters used in the computation. In both the reduced pressure flames of Fenimore & Jones (1959) and Vandooren *et al.* (1975) almost the sole chemical contribution of the carbon monoxide is by way of reaction (xxi).

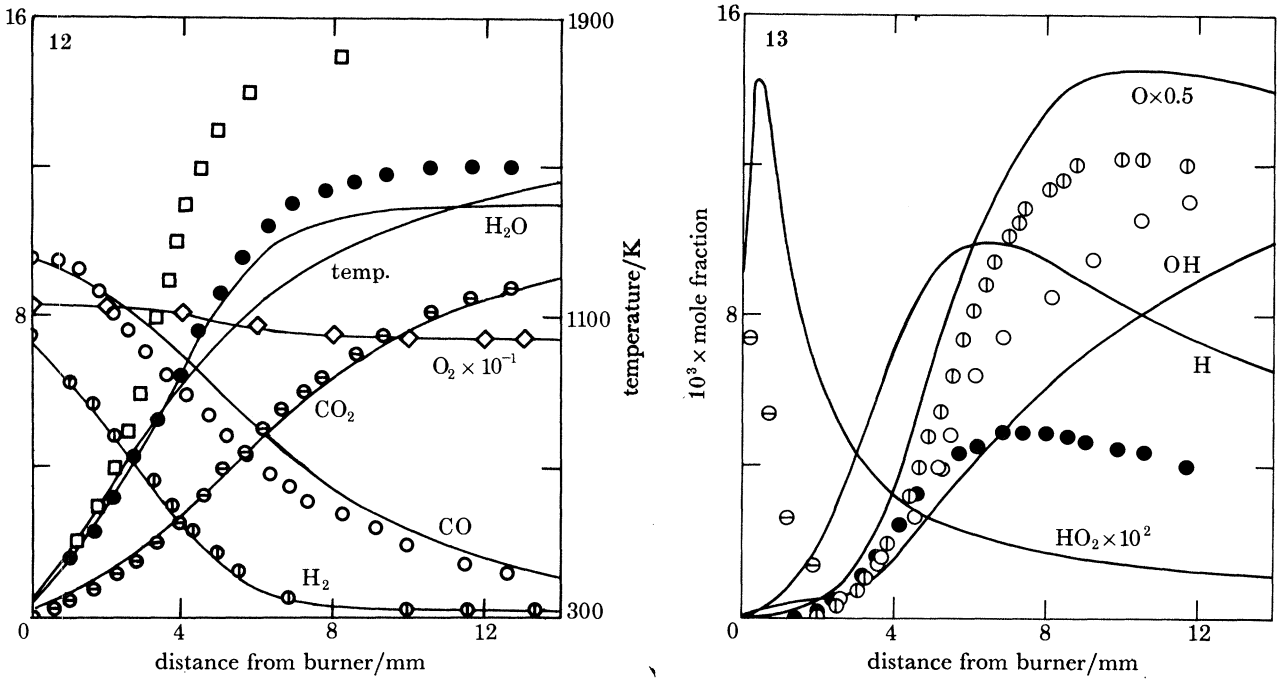

FIGURE 12. Profiles of temperature and mole fractions of stable species against distance from burner in a lean hydrogen–carbon monoxide–oxygen flame, comparing computed lines with points representing observations of Vandooren *et al.* (1975). Mole fraction composition of supply mixture was: $X_{H_2} = 0.114$, $X_{CO} = 0.094$ and $X_{O_2} = 0.792$, with $p = 5.32$ kPa (40 Torr). Flow velocity of fresh gas was 63.7 cm s^{-1}, measured for gas at 298 K and 5.32 kPa. Transport parameters for computation are from table 1. Reaction rate parameters are as in set F, table 4. Points: □, temperature; ○, CO; ⊙, H_2; ◇, $0.1 \times O_2$; ⊖, CO_2; ●, H_2O.

FIGURE 13. Profiles of mole fractions of radicals against distance from burner for flame of figure 12, comparing computed lines with points representing observations of Vandooren *et al.* (1975). Transport parameters for computations are from table 1. Reaction rate parameters are as in set F, table 4. Points: ●, H; ○, OH; ⊙, 0.5×0; ⊖, $10^2 \times HO_2$.

4. Discussion

(*a*) *Flame mechanism*

The major conclusion from the numerical investigation is that the premixed flame velocities and properties of the whole range of hydrogen–carbon monoxide–oxygen–nitrogen mixtures, and carbon monoxide–oxygen–nitrogen mixtures containing small quantities of water vapour, may be very largely accommodated by changes in purely physical effects like the thermal conductivities and diffusional properties of the mixtures, plus the addition of the single reaction (xxi) to the kinetic mechanism responsible for hydrogen–oxygen–nitrogen flames. Within the limits of experimental error, table 4 shows this conclusion to be entirely valid in the less fuel-rich flames considered there, containing 40 % (H_2 + CO) in the initial mixture. It is less valid in the flames containing 60 % (H_2 + CO) initially, and in these flames (and the low temperature flames discussed in §3 (*a*)) an additional chain-terminating effect from reaction (xxiii) appears to modify the simple picture. Reaction (xxii), on the other hand, has little

influence on the burning velocities of any of the mixtures. The reasons for these findings, and for the decrease in burning velocity as the hydrogen–carbon monoxide mixtures become progressively weaker in hydrogen, become clear from an examination of the flame structures.

Figures 14, 16 and 18 show the computed profiles of the temperature and the mole fractions of the stable species and hydrogen atoms in flames C, J and F of table 4, for the runs in which

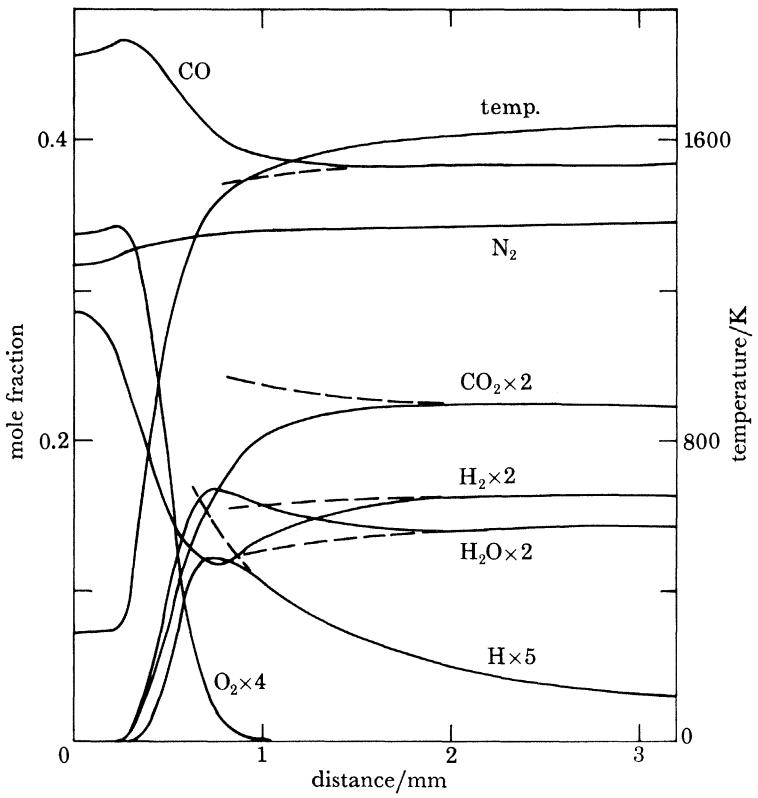

FIGURE 14. Computed temperature profile and mole fraction profiles for stable species and hydrogen atoms in 60 % (24.1 % hydrogen + 75.9 % carbon monoxide) + 40 % air flame at atmospheric pressure, with T_u = 298 K. Transport parameters are from table 1. Reaction rate parameters are as in set F, table 4. Computed burning velocity $S_{u,calc}$ = 94.6 cm s^{-1}, referred to unburned gas at 298 K and 101 kPa. Solid lines, complete flame calculation; broken lines, calculation with partial equilibrium assumptions on reactions (i), (ii), (iii) and (xxi).

set F of rate parameters was used. Figures 15, 17 and 19 show the mole fractions of the radical species from the same computations. Figures 20 and 21 show similar sets of profiles for a flame with initial composition as for flame F, but with 2.3 % of the total mixture consisting of water vapour in place of an equivalent mole fraction of nitrogen. Figures 22 and 23 show the profiles for an initial mixture having the same fuel composition as flame C, but with 70 % fuel + air. This flame has a lower final temperature than flame C. In each figure the solid lines show the results of the complete flame calculations, while the broken lines show profiles calculated by applying the composite flux method of Dixon-Lewis *et al.* (1975), with partial equilibrium assumptions on reactions (i), (ii), (iii) and (xxi), to the recombination regions on the hot sides of the flames. Several interesting features emerge.

(i) In all the fuel-rich flames having mixtures of hydrogen and carbon monoxide as fuel, the water profile shows a maximum near or just before the maximum in the hydrogen atom

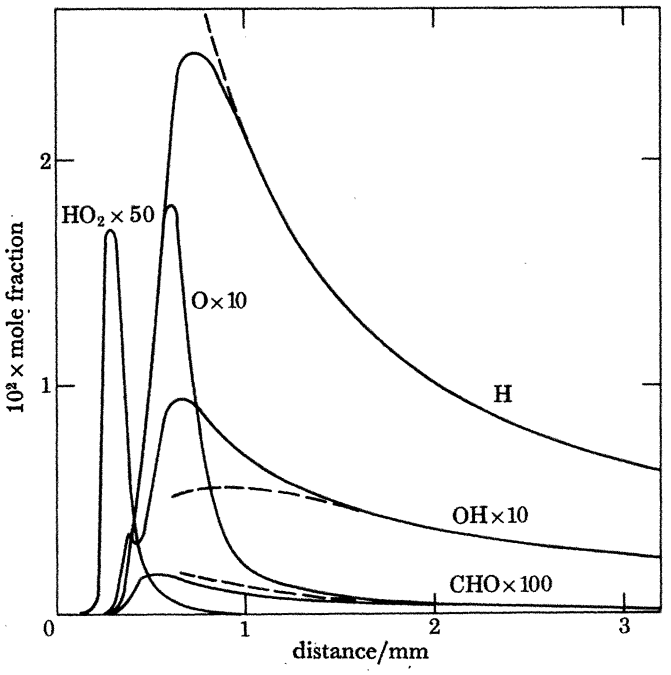

FIGURE 15. Computed mole fraction profiles for radical species in 60% (24.1% hydrogen + 75.9% carbon monoxide) + 40% air flame at atmospheric pressure, with $T_u = 298$ K. Transport parameters are from table 1. Reaction rate parameters are as in set F, table 4. Same distance zero as in figure 14. Solid lines, complete flame calculation; broken lines for H, OH and O, calculation with partial equilibrium assumptions on reactions (i), (ii), (iii) and (xxi).

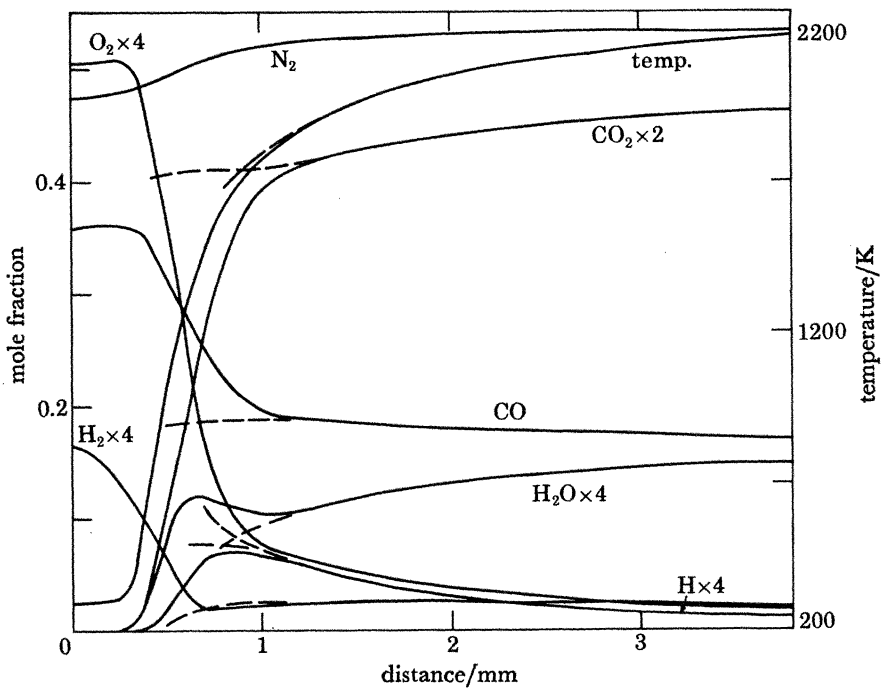

FIGURE 16. Computed temperature profile and mole fraction profiles for stables species and hydrogen atoms in 40% (10.5% hydrogen + 89.5% carbon monoxide) + 60% air flame at atmospheric pressure, with $T_u = 298$ K. Transport parameters are from table 1. Reaction rate parameters are as in set F, table 4. Computed burning velocity $S_{u,calc} = 69.1$ cm s^{-1}, referred to unburned gas at 298 K and 101 kPa. Solid lines, complete flame calculation; broken lines, calculation with partial equilibrium assumptions on reactions (i), (ii), (iii) and (xxi).

PHILOSOPHICAL TRANSACTIONS OF THE ROYAL SOCIETY A MATHEMATICAL, PHYSICAL & ENGINEERING SCIENCES

profile (see figures 14, 16, 18, 20 and 22). There is thus a water overshoot in the reaction zones of all the flames. This overshoot is a 'kinetic overshoot', in that it is associated with the higher rate coefficient of reaction (i) compared with reaction (xxi) in the major part of the reaction zone. The hydrogen is preferentially oxidized in such a way that reaction (i) reaches a (partial) equilibrium condition at a temperature below the final flame temperature. Because of the effect of temperature on its equilibrium constant, reaction (i) may then proceed in the reverse direction as the temperature rises further, with the hydroxyl radicals produced by

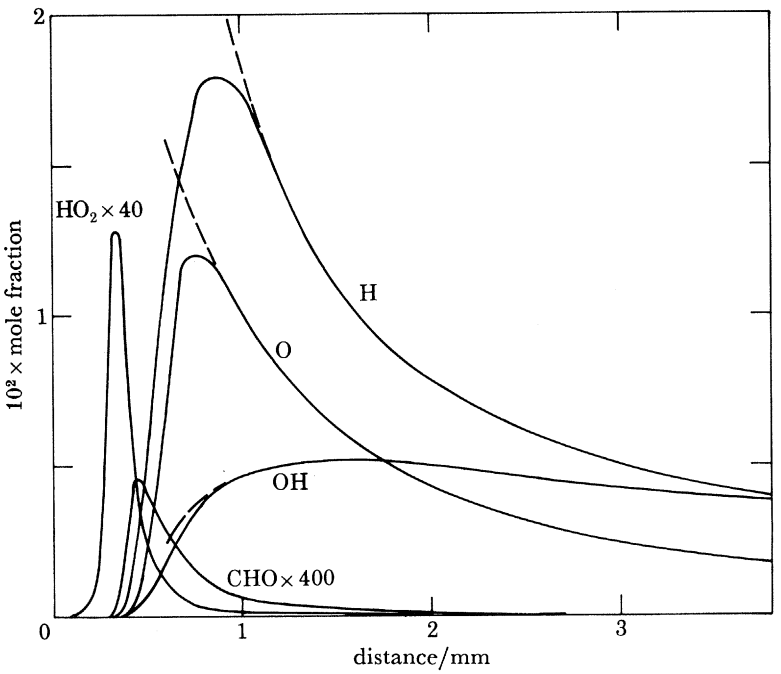

FIGURE 17. Computed mole fraction profiles for radical species in 40 % (10.5 % hydrogen + 89.5 % carbon monoxide) + 60 % air flame at atmospheric pressure, with $T_u = 298$ K. Transport parameters are from table 1. Reaction rate parameters are as in set F, table 4. Same distance zero as in figure 16. Solid lines, complete flame calculation; broken lines for H, OH and O, calculation with partial equilibrium assumptions on reactions (i), (ii), (iii) and (xxi).

reaction (−i) going to complete the oxidation of the carbon monoxide via reaction (xxi). A significant part of the conversion of carbon monoxide to carbon dioxide in the flames is thus in effect a water gas shift reaction. On account of the slower rate of reaction (xxi) compared with reaction (i), the full water gas equilibrium, and hence the partial equilibrium condition, is not achieved until after the water overshoot has subsided.

(ii) The establishment of the partial equilibrium condition occurs more rapidly in hotter flames. In flame C (containing 60 % fuel), figures 14 and 15 show that the water gas equilibrium is established at about 1.8 mm after the position of first appreciable temperature rise, or at about 1.3 mm after the maximum in the hydrogen atom concentration. The temperature over most of the 1.3 mm interval lies between 1500 and 1600 K. In the flame containing 70 % fuel (figures 22 and 23), on the other hand, the maximum temperature achieved within the whole distance range shown is 1360 K. The water gas equilibrium is not established within this range, which extends for about 5 mm downstream of the position of maximum hydrogen atom concentration. Attention has already been drawn in §§ 3(*a*) and 3(*c*) to an even slower

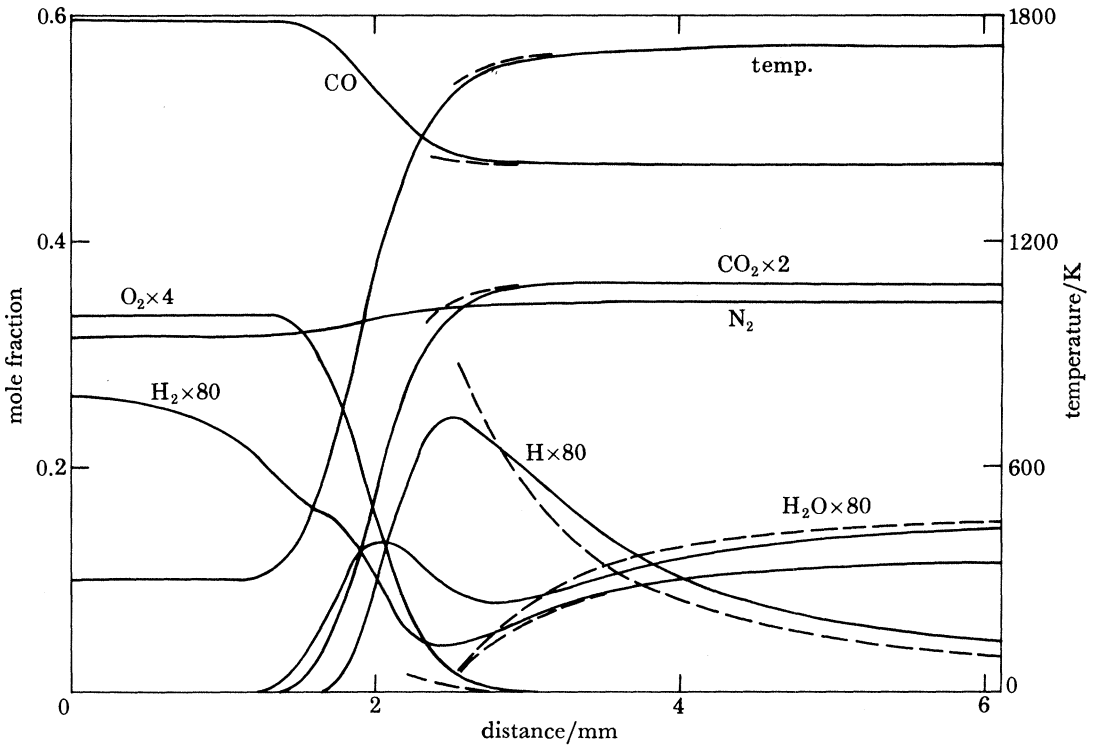

FIGURE 18. Computed temperature profile and mole fraction profiles for stable species and hydrogen atoms in dry 60 % (0.55 % hydrogen + 99.45 % carbon monoxide) + 40 % air flame at atmospheric pressure, with T_u = 298 K. Transport parameters are from table 1. Reaction rate parameters are as in set F, table 4. Computed burning velocity $S_{u,calc}$ = 19.5 cm s^{-1}, referred to unburned gas at 298 K and 101 kPa. Solid lines, complete flame calculation; broken lines, calculation with partial equilibrium assumptions on reactions (i), (ii), (iii) and (xxi).

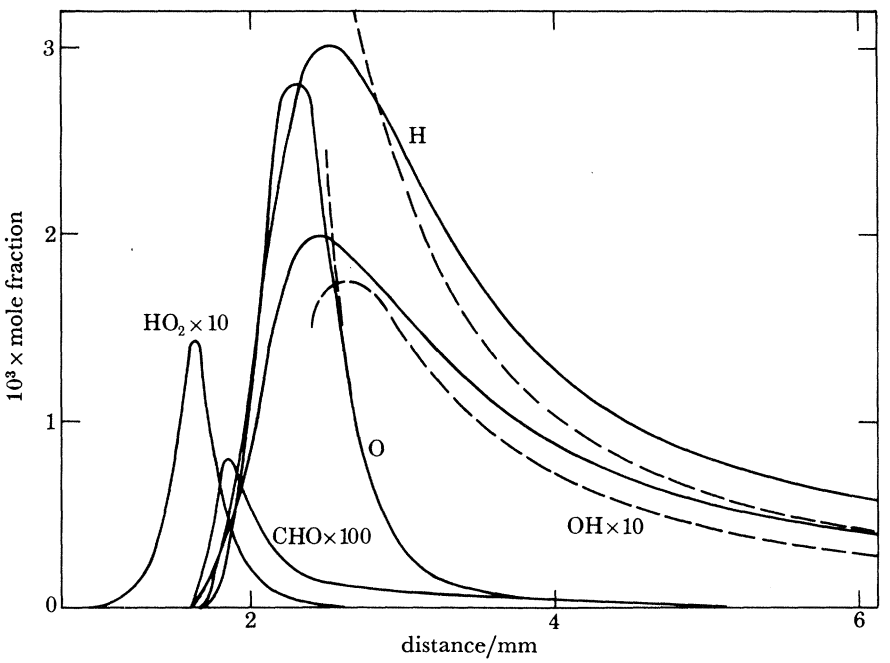

FIGURE 19. Computed mole fraction profiles for radical species in dry 60 % (0.55 % hydrogen + 99.45 % carbon monoxide) + 40 % air flame at atmospheric pressure, with T_u = 298 K. Transport parameters are from table 1. Reaction rate parameters are as in set F, table 4. Same distance zero as in figure 18. Solid lines, complete flame calculation; broken lines for H, OH and O, calculation with partial equilibrium assumptions on reactions (i), (ii), (iii) and (xxi).

approach to the water gas equilibrium in a flame having a final temperature of 1100 K. Because of the slow approach to the water gas equilibrium, the partial equilibrium situation is not rapidly established in the burnt gas of hydrogen–carbon monoxide–air flames having final temperatures below about 1500 K. In such situations the rates of reactions (−i) and (xxi) determine the progress of the oxidation of the carbon monoxide. The reaction systems

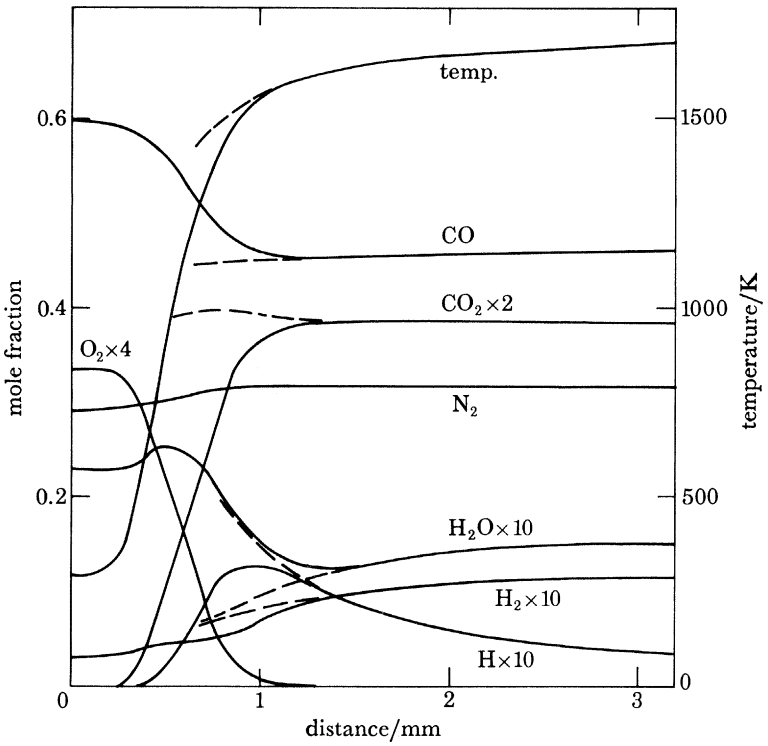

FIGURE 20. Computed temperature profile and mole fraction profiles for stable species and hydrogen atoms in moist 60 % (0.55 % hydrogen + 99.45 % carbon monoxide) + 40 % air flame at atmospheric pressure, with T_u = 298 K. Initial mixture contained 2.30 % water vapour in place of an equivalent quantity of nitrogen in dry mixture. Transport parameters are from table 1. Reaction rate parameters are as in set F, table 4. Computed burning velocity $S_{u,calc}$ = 44.7 cm s^{-1}, referred to unburned gas at 298 K and 101 kPa. Solid lines, complete flame calculation; broken lines, calculation with partial equilibrium assumptions on reactions (i), (ii), (iii) and (xxi).

(i) and (xxi) remain displaced from their equilibrium positions over an appreciable region of the burnt gas, and in some circumstances this may further cause freezing of the eventual combustion products at a non-equilibrium composition.

(iii) The final stage of the reaction in any flame is the decay of the radical pool. Most of this decay in the hotter flames considered here (T_b > 1500 K) follows the achievement of partial equilibrium of reactions (i), (ii), (iii) and (xxi). In flames at the richer end of this hotter range there is virtually no molecular oxygen remaining after the partial equilibrium is established, and little further oxidation of carbon monoxide occurs. However, in the even hotter fuel-rich and fuel-lean flames not far from stoichiometric, there is still appreciable molecular oxygen available in the recombination region. A slow oxidation of additional carbon monoxide takes place during the decay of the radical pool in these flames, along with some further oxidation of hydrogen. The effect is illustrated in figure 16, which refers to flame J containing 40 % (H_2 + CO) + 60 % air initially.

(iv) In the flames containing much hydrogen, the chain branching process that separates the unpaired electron spins of the oxygen molecules occurs essentially in the same way as when carbon monoxide is absent, that is, by way of reaction (ii) in association with (i) and (iii). These reactions normally achieve partial equilibrium very soon after the attainment of the maximum hydrogen atom concentrations in the flames (Dixon-Lewis 1979). This same approach to partial equilibrium of reactions (i), (ii) and (iii) is still the driving force when only trace quantities of hydrogen or water are present in carbon monoxide–oxygen–nitrogen flames; with the difference that the hydrogen–oxygen system reactions do not then themselves

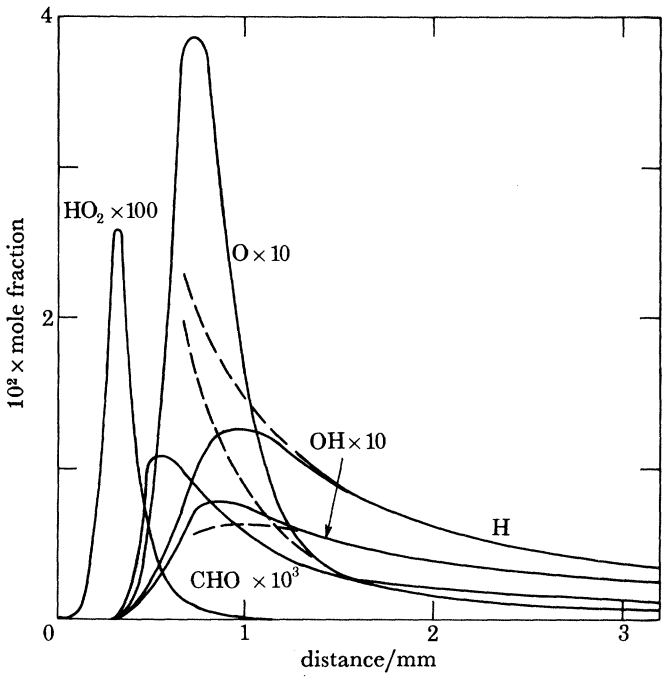

FIGURE 21. Computed mole fraction profiles for radical species in moist 60 % (0.55 % hydrogen + 99.45 % carbon monoxide) + 40 % air flame at atmospheric pressure, with $T_u = 298$ K. Initial mixture contained 2.30 % water vapour in place of an equivalent quantity of nitrogen in dry mixture. Transport parameters are from table 1. Reaction rate parameters are as in set F, table 4. Same distance zero as in figure 20. Solid lines, complete flame calculation; broken lines for H, OH and O, calculation with partial equilibrium assumptions on reactions (i), (ii), (iii) and (xxi).

contribute appreciably to the temperature rise, but merely complete the cycle in which carbon monoxide is oxidized by reaction (xxi). However, in these flames containing only small quantities of hydrogenous material, the hydrogen content of the radical pool may at its maximum be comparable with or greater than that of the remaining *molecular* hydrogen-containing species. In these circumstances the constraint on the overall hydrogen content will combine with the partial equilibrium conditions on reactions (i), (ii), and (iii) or (xviii), so as to enrich the radical pool in oxygen atoms, and perhaps to limit its size. These effects are shown by the data in table 6, which gives the maximum mole fractions of H, O and OH for each of the runs of table 4, together with the mole fractions of O, OH, H_2 and H_2O at the positions of maximum mole fraction of atomic hydrogen. The effects are also shown over the complete flames by a comparison of the profiles in figures 15, 17, 19, 21 and 23.

As a result of the constraints, the oxygen atoms in flames with little hydrogenous material

have a low effective reactivity by all reactions other than (xxii), and in the absence of reaction (xxii) they merely accumulate into a large pool (flames F and L, set D, in table 6). Interesting consequences of this are, first, the well known intensification of the brilliant blue colour of the flames as their content of hydrogenous material is severely reduced (the blue colouring being directly associated with the occurrence of reaction (xxii)); and secondly, the small effect of reaction (xxii) on the computed burning velocities. Reaction (xxii) also has little effect in the flames containing higher proportions of hydrogen, since it cannot then compete successfully with reaction (iii).

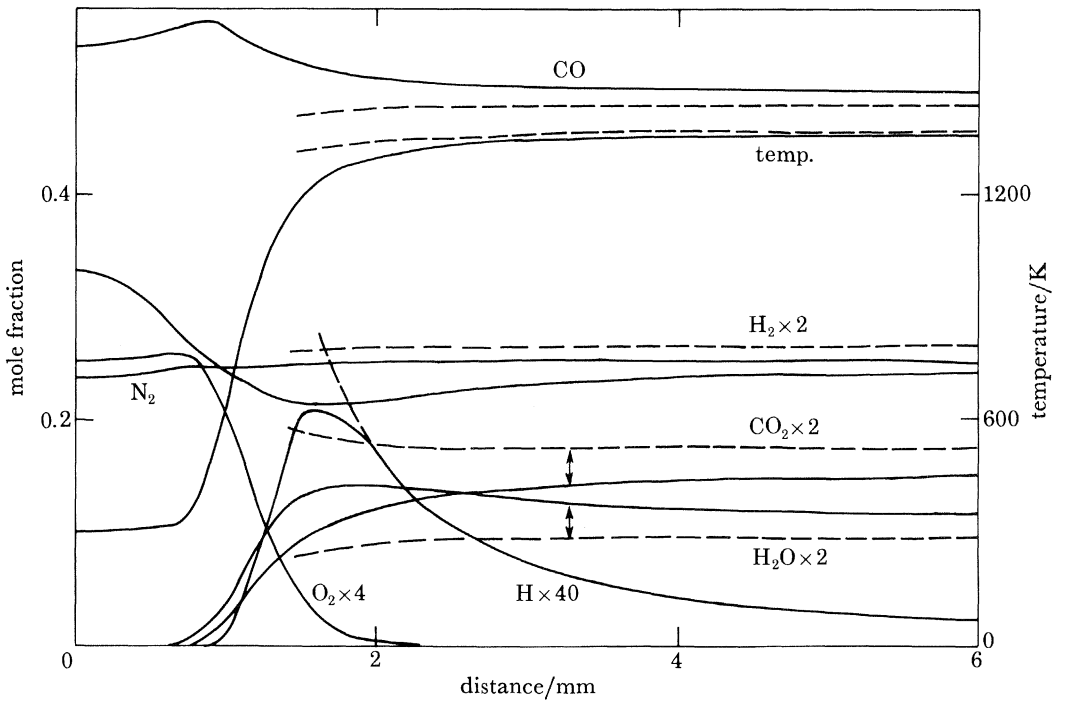

FIGURE 22. Computed temperature profile and mole fraction profiles for stable species and hydrogen atoms in 70% (24.1% hydrogen + 75.9% carbon monoxide) + 30% air flame at atmospheric pressure, with T_u = 298 K. Transport parameters are from table 1. Reaction rate parameters are as in set F, table 4. Computed burning velocity $S_{u,calc}$ = 30.3 cm s^{-1}, referred to unburned gas at 298 K and 101 kPa. Solid lines, complete flame calculation; broken lines, calculation with partial equilibrium assumptions on reactions (i), (ii), (iii) and (xxi).

The effect of the low reactivity of oxygen atoms by reactions other than (xxii) in the flames containing only traces of hydrogen or water vapour is shown particularly strongly by the results for flame L of tables 4 and 6. In the computation of this flame the omission of the chain terminating steps (xxii) and (xxiii) as in set D causes a small *reduction* in the predicted burning velocity. The situation in run D, flame L, is that the part of the radical pool consisting of H, O and OH builds up to much higher concentrations in the main reaction zone than occurs in runs E and F. However, near the maximum overall radical concentration, reactions (i), (ii) and (iii) will be moving towards their partial equilibrium positions; and because of the constraints imposed by the partial equilibrium conditions, the proportion of hydroxyl radicals in the pool, and even their absolute concentration, becomes lower in the main reaction zone of run D. The carbon monoxide is then not oxidized so rapidly or completely in this

reaction zone, the temperature corresponding with the peak radical concentration is lower, and the flame velocity becomes smaller.

(v) For the whole range of hydrogen–carbon monoxide–air flames, a further consequence of the oxygen atom (and hydroxyl radical) enrichment shown in table 6 is the movement of the position of maximum burning velocity towards richer fuel–air mixtures as the proportion of carbon monoxide in the fuel is increased. This effect is associated with the increased prominence given in the less rich flames to the chain-terminating reactions (xiii) and (xiv).

(vi) Moving from left to right in figures 16 and 18 (from cold to hot in the flames), much of the hydrogen is oxidized to water quite early in the reaction zones, and in each case the maximum in the water profile appears at a position upstream of the maximum hydrogen atom concentration. During the decrease in water concentration immediately following the maximum, some of the water contributes to the hydrogenated species in the radical pool

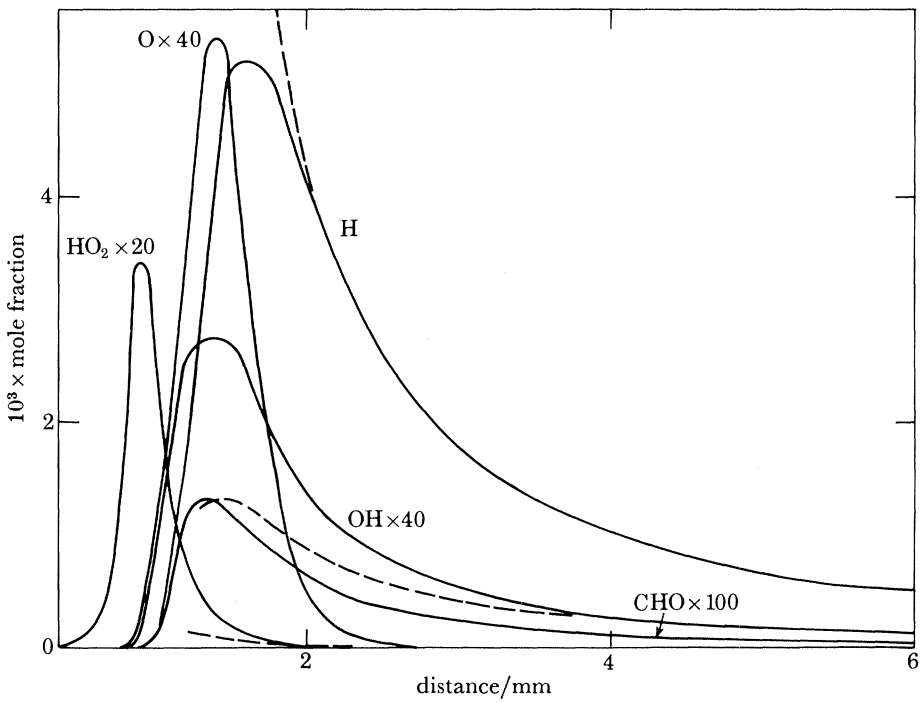

FIGURE 23. Computed mole fraction profiles for radical species in 70% (24.1% hydrogen + 75.9% carbon monoxide) + 30% air flame at atmospheric pressure, with T_u = 298 K. Transport parameters are from table 1. Reaction rate parameters are as in set F, table 4. Same distance zero as in figure 22. Solid lines, complete flame calculation; broken lines for H, OH and O, calculation with partial equilibrium assumptions on reactions (i), (ii), (iii) and (xxi).

by way of reaction (−xviii). Then, on the downstream side of the maximum hydrogen atom concentration, the water concentration and the molecular hydrogen concentration gradually increase as the gases pass through the recombination region towards full equilibrium. It is noteworthy that the partial equilibrium conditions appear to apply in the recombination zones of flames C and J (figures 14–17), as well as in the flame of figures 20 and 21. They do not, however, appear to apply in flame F (figures 18 and 19). Flame F contains much less hydrogenous material than any of the other three, and at the maximum size of the radical pool the mole fraction ratio X_{H_2}/X_{CO} is only about 10^{-3}. As a result there is probably at this

TABLE 6. COMPUTED MOLE FRACTIONS OF H, O, OH, H_2 AND H_2O, AND THE TEMPERATURE, AT THE POSITION OF MAXIMUM HYDROGEN ATOM CONCENTRATION IN RUNS OF TABLE 4, TOGETHER WITH MAXIMUM MOLE FRACTIONS OF OXYGEN ATOMS AND HYDROXYL RADICALS IN THE FLAMES

flame		set D	set E	set F
A	$S_{u,calc}/(cm\ s^{-1})$	170	170	170
	$10^2\ X_{H,max}$	3.59	3.59	3.59
	$10^4\ X_O$	1.63	1.63	1.63
	$10^4\ X_{OH}$	3.08	3.08	3.08
	X_{H_2}	0.4472	0.4472	0.4472
	X_{H_2O}	0.1711	0.1711	0.1711
	T/K	1343	1343	1343
	$10^4\ X_{O,max}$	4.50	4.50	4.50
	$10^4\ X_{OH,max}$	3.35	3.35	3.35
B	$S_{u,calc}/(cm\ s^{-1})$	148.4	148.0	136.7
	$10^2\ X_{H,max}$	> 3.46	> 3.45	3.00
	$10^4\ X_O$	2.60	2.60	3.04
	$10^4\ X_{OH}$	4.37	4.36	4.24
	X_{H_2}	0.2708	0.2712	0.2743
	X_{H_2O}	0.1545	0.1543	0.1519
	T/K	1345	1347	1350
	$10^4\ X_{O,max}$	6.39	6.32	5.83
	$10^4\ X_{OH,max}$	4.74	4.72	4.38
C	$S_{u,calc}/(cm\ s^{-1})$	113.9	112.2	94.6
	$10^2\ X_{H,max}$	3.57	3.42	2.50
	$10^4\ X_O$	12.0	11.3	9.33
	$10^4\ X_{OH}$	10.5	10.3	9.23
	X_{H_2}	0.0554	0.0565	0.0591
	X_{H_2O}	0.0834	0.0829	0.0848
	T/K	1380	1388	1421
	$10^4\ X_{O,max}$	22.6	21.2	17.8
	$10^4\ X_{OH,max}$	11.4	11.0	9.23
D	$S_{u,calc}/(cm\ s^{-1})$	87.9	84.6	73.3
	$10^2\ X_{H,max}$	3.32	2.86	2.09
	$10^4\ X_O$	19.3	15.2	14.5
	$10^4\ X_{OH}$	9.94	9.71	9.06
	X_{H_2}	0.0202	0.0213	0.0214
	X_{H_2O}	0.0316	0.0330	0.0338
	T/K	1435	1464	1475
	$10^4\ X_{O,max}$	46.3	37.9	30.1
	$10^4\ X_{OH,max}$	11.6	11.2	10.4
E	$S_{u,calc}/(cm\ s^{-1})$	—	—	44.7
	$10^2\ X_{H,max}$	—	—	1.19
	$10^4\ X_O$	—	—	30.1
	$10^4\ X_{OH}$	—	—	6.25
	X_{H_2}	—	—	0.0044
	X_{H_2O}	—	—	0.0086
	T/K	—	—	1513
	$10^4\ X_{O,max}$	—	—	40.4
	$10^4\ X_{OH,max}$	—	—	6.25
F	$S_{u,calc}/(cm\ s^{-1})$	22.7	20.7	19.5
	$10^2\ X_{H,max}$	0.613	0.323	0.300
	$10^4\ X_O$	111.4	21.7	17.8
	$10^4\ X_{OH}$	1.40	2.05	1.94
	$10^4\ X_{H_2}$	0.812	4.59	5.17
	$10^4\ X_{H_2O}$	1.47	10.5	11.4
	T/K	1461	1594	1588
	$10^4\ X_{O,max}$	127.7	29.8	27.3
	$10^4\ X_{OH,max}$	2.56	2.05	1.97

PHILOSOPHICAL TRANSACTIONS OF THE ROYAL SOCIETY A MATHEMATICAL, PHYSICAL & ENGINEERING SCIENCES

TABLE 6 (*cont.*)

flame		set D	set E	set F
G	$S_{u,calc}/(cm\ s^{-1})$	265	265	265
	$10^2\ X_{H,max}$	7.52	7.52	7.52
	$10^4\ X_O$	30.8	30.8	30.8
	$10^4\ X_{OH}$	50.9	50.9	50.9
	X_{H_2}	0.1507	0.1507	0.1507
	X_{H_2O}	0.2480	0.2480	0.2480
	T/K	1550	1550	1550
	$10^4\ X_{O,max}$	45.8	45.8	45.8
	$10^4\ X_{OH,max}$	60.0	60.0	60.0
H	$S_{u,calc}/(cm\ s^{-1})$	203	202	203
	$10^2\ X_{H,max}$	5.60	5.59	> 5.45
	$10^4\ X_O$	58.9	60.0	60.6
	$10^4\ X_{OH}$	75.9	73.9	70.7
	X_{H_2}	0.0660	0.0666	0.0690
	X_{H_2O}	0.2041	0.2027	0.1994
	T/K	1613	1599	1582
	$10^4\ X_{O,max}$	66.3	65.8	64.8
	$10^4\ X_{OH,max}$	84.0	83.9	84.2
I	$S_{u,calc}/(cm\ s^{-1})$	109.0	108.3	108.0
	$10^2\ X_{H,max}$	3.16	2.96	2.89
	$10^4\ X_O$	111.2	97.1	100.3
	$10^4\ X_{OH}$	58.4	64.9	62.8
	X_{H_2}	0.0147	0.0159	0.0152
	X_{H_2O}	0.0714	0.0700	0.0715
	T/K	1594	1689	1661
	$10^4\ X_{O,max}$	111.2	107.5	103.8
	$10^4\ X_{OH,max}$	73.8	72.9	72.9
J	$S_{u,calc}/(cm\ s^{-1})$	72.0	71.1	69.1
	$10^2\ X_{H,max}$	2.26	> 1.87	1.80
	$10^4\ X_O$	132.2	111.7	114.6
	$10^4\ X_{OH}$	40.6	42.7	39.3
	X_{H_2}	0.0058	0.0058	0.0055
	X_{H_2O}	0.0249	0.0263	0.0276
	T/K	1637	1700	1645
	$10^4\ X_{O,max}$	138.8	121.7	114.6
	$10^4\ X_{OH,max}$	53.1	51.8	51.6
K	$S_{u,calc}/(cm\ s^{-1})$	—	—	40.6
	$10^2\ X_{H,max}$	—	—	0.762
	$10^4\ X_O$	—	—	123.3
	$10^4\ X_{OH}$	—	—	18.5
	$10^4\ X_{H_2}$	—	—	11.0
	$10^4\ X_{H_2O}$	—	—	59.0
	T/K	—	—	1668
	$10^4\ X_{O,max}$	—	—	123.3
	$10^4\ X_{OH,max}$	—	—	26.4
L	$S_{u,calc}/(cm\ s^{-1})$	19.0	20.0	19.6
	$10^2\ X_{H,max}$	0.321	0.156	0.155
	$10^4\ X_O$	220.3	81.0	84.6
	$10^4\ X_{OH}$	3.70	7.03	6.11
	$10^4\ X_{H_2}$	0.517	1.06	0.993
	$10^4\ X_{H_2O}$	2.27	6.55	6.74
	T/K	1555	1870	≈ 1780
	$10^4\ X_{O,max}$	220.3	82.0	84.6
	$10^4\ X_{OH,max}$	9.56	8.73	> 8.49

stage a very small overshoot in the carbon dioxide concentration, following which the oxygen-deficient radical pool gives essentially molecular hydrogen during its recombination. A rather slow rate of oxidation of the latter by the water gas shift reactions could then account for the computed small departure from partial equilibrium.

Because of this small departure from partial equilibrium the distance scales for the profiles from the partial equilibrium and full flame calculations cannot be matched precisely in figures 18 and 19. As drawn, the partial equilibrium profiles (including those regions that are apparently coincident with the solid lines) are probably in an extreme left position. The validity of this position is doubtful, since according to figure 19 it implies an appreciable overshoot in the total radical concentration. If the partial equilibrium profiles are all moved somewhat to the right, for example by about 0.25 mm, it is possible to eliminate most of this overshoot in the total pool, and at the same time to arrange for the small disequilibrium between hydrogen and water to be shared between their two profiles.

(vii) The computed burning velocity of the water-containing initial mixture of figures 20 and 21 is exactly the same as the burning velocity of flame E in tables 4 and 6. As a fraction of the total mixture, flame E contains 1.80 % hydrogen initially, while the water-containing mixture has 0.33 % hydrogen and 2.30 % water. The hydrogen is thus about 1.5 times as efficient a catalyst as the added water vapour. Figure 20 shows that even when the initial mixture contains considerable water, some further water is still formed in the reaction before its subsequent dissociation to form the radical pool. Apart from minor differences associated with the slightly increased initial carbon monoxide and total elemental hydrogen content of the water-containing flame compared with flame E, the two flames achieve the same partial equilibrium composition not long after the maximum hydrogen atom concentration. Comparison of the radical profiles in figure 21 with the data given for flame E in table 6 shows that the maximum sizes of the two radical pools, and their distribution between H, OH and O at the maxima, are almost the same. In fact the water-containing flame has slightly higher hydroxyl radical concentrations than flame E, and it has to achieve in the same time a total of approximately 10 % more production of carbon dioxide by reaction (xxi) to establish the final water gas equilibrium. The maximum oxygen atom concentrations in the two flames were also very nearly the same, and this applied additionally to the complete series of 60 % fuel + air flames belonging to curves 2, 3 and 4 in figure 6. The maximum hydrogen atom and hydroxyl radical concentrations in these latter flames decreased as the initial water content was made smaller.

It is probable that the reduced catalytic efficiency of water vapour compared with that of hydrogen is associated with its lower molar free energy. The chain branching cycle that produces the radical pool in the water–oxygen containing mixtures necessitates an attack of either hydrogen or oxygen atoms on water vapour, by reaction (−i) or (−xviii). Both reactions have activation energies of approximately 75 kJ mol^{-1}, and this makes radical production more difficult than in hydrogen–oxygen containing mixtures. In the latter the pair of free electron spins associated with the oxygen atom is more easily separated by a direct occurrence of reaction (iii) alone.

(*b*) *Reaction rate parameters*

By means of the present study it was initially hoped that, in addition to establishing the flame mechanism, it would be possible to deduce information about the rate coefficients of

several reactions involving carbon monoxide and the formyl radical in the flames. It has turned out, however, that the burning velocities measured by Jahn (1934), Badami & Egerton (1955), Scholte & Vaags (1959*b*, *c*) and Wires *et al.* (1959) can be very largely explained by the addition of reaction (xxi) alone to the hydrogen–oxygen–nitrogen flame reaction mechanism. As the data in table 6 show, the contribution of reaction (xxii) to the flame velocity is always small. Reaction (xxiii) combined with the subsequent reactions of the formyl radical contributes a somewhat larger chain terminating effect in certain flames, but the available evidence is not sufficient for a full quantitative interpretation. On the assumptions that $k_{23,H_2} = 5 \times 10^{14}$ exp $(-755/T)$ and $k_{-23,H_2} = 3 \times 10^{14}$ exp $(-7835/T)$, k_{25} should lie within the limits $k_{25} = (4 \pm 1) \times 10^{13}$ cm^3 mol^{-1} s^{-1}. The three combinations of k_{24} and k_{25} given as sets 2A, 2B and 2C in table 3 are all able to model the complete range of burning velocity data within the experimental error, leading to $k_{24} = 3 \times 10^{(12\pm1)}$.

The observations of Baldwin & Cowe (1962) on the inhibitory effect of formaldehyde on the second explosion limit of the hydrogen–oxygen–nitrogen system in a potassium chloride coated vessel at 813 K are also relevant to the discussion of k_{24}. Their results could only be explained on the basis that, in a mixture having the mole fractions 0.28, 0.07 and 0.65 of hydrogen, oxygen and nitrogen respectively, reaction (xxiv) is at least twenty times as fast as reaction (−xxiii). For the value of k_{-23} given above, this leads to $k_{24} \geqslant 3 \times 10^{11}$ cm^3 mol^{-1} s^{-1} at 813 K.

We thank the Science Research Council for the award of a Post-doctoral Fellowship to M.A.C. The support of British Gas during the early stages of the work is also gratefully acknowledged.

References

Badami, G. N. & Egerton, Sir A. 1955 *Proc. R. Soc. Lond.* A **228**, 297.
Baldwin, R. R. & Cowe, D. W. 1962 *Trans. Faraday Soc.* **58**, 1768.
Baldwin, R. R., Jackson, D., Melvin, A. & Rossiter, B. N. 1972 *Int. J. chem. Kinet.* **4**, 277.
Baulch, D. L. & Drysdale, D. D. 1974 *Combust. Flame* **23**, 215.
Baulch, D. L., Drysdale, D. D., Duxbury, J. & Grant, S. J. 1976 *Evaluated kinetic data for high temperature reactions*, vol. 3. London: Butterworth.
Boularas, R., Sullivan, E. & Dixon-Lewis, G. 1981 To be published.
Buckler, E. J. & Norrish, R. G. W. 1938 *Proc. R. Soc. Lond.* A **167**, 292, 318.
Del Greco, F. P. & Kaufman, F. 1963 *9th Int. Symp. Combust.*, p. 659. New York: Academic Press.
Dixon-Lewis, G. 1968 *Proc. R. Soc. Lond.* A **307**, 111.
Dixon-Lewis, G. 1972 *Proc. R. Soc. Lond.* A **330**, 219.
Dixon-Lewis, G. 1979 *Phil. Trans. R. Soc. Lond.* A **292**, 45.
Dixon-Lewis, G., Goldsworthy, F. A. & Greenberg, J. B. 1975 *Proc. R. Soc. Lond.* A **346**, 261.
Dixon-Lewis, G. & Isles, G. L. 1969 *Proc. R. Soc. Lond.* A **308**, 517.
Dixon-Lewis, G. & Linnett, J. W. 1953 *Trans. Faraday Soc.* **49**, 756.
Dixon-Lewis, G., Sutton, M. M. & Williams, A. 1965 *Trans. Faraday Soc.* **61**, 255.
Dixon-Lewis, G. & Williams, D. J. 1977 *Comprehensive chemical kinetics* (ed. C. H. Bamford & C. F. H. Tipper), vol. 17, p. 1. Amsterdam: Elsevier.
Edmondson, H. & Heap, M. P. 1971 *Combust. Flame* **16**, 161.
Fenimore, C. P. & Jones, G. W. 1959 *J. phys. Chem.* **63**, 1154.
Fletcher, R. A. & Pilcher, G. 1970 *Trans. Faraday Soc.* **66**, 794.
Friedman, R. & Burke, E. 1954 *J. chem. Phys.* **22**, 824.
Friedman, R. & Cyphers, J. A. 1955 *J. chem. Phys.* **23**, 1875.
Fristrom, R. M. & Westenberg, A. A. 1957 *Combust. Flame* **1**, 217.
Günther, R. & Janisch, G. 1971 *Chemie-Ingr-Tech.* **43**, 975.
Jahn, G. 1934 *Der Zundvorgang in Gasgemischen.* Berlin: Oldenbourg.
JANAF 1971 *Thermochemical tables* (2nd edn). National Bureau of Standards Publication NSRDS-NBS 37, Washington, D.C.

PHILOSOPHICAL TRANSACTIONS OF THE ROYAL SOCIETY A MATHEMATICAL, PHYSICAL & ENGINEERING SCIENCES

JANAF 1974 *Thermochemical tables supplement. J. phys. chem. Ref. Data* **3**, 311.
Mack, G. P. R. & Thrush, B. A. 1973 *J. chem. Soc. Faraday Trans.* I **69**, 208.
Mason, E. A. & Monchick, L. 1962 *J. chem. Phys.* **36**, 1622.
Monchick, L. & Mason, E. A. 1961 *J. chem. Phys.* **35**, 1676.
Monchick, L., Munn, R. J. & Mason, E. A. 1966 *J. chem. Phys.* **45**, 3051.
Monchick, L., Pereira, A. N. G. & Mason, E. A. 1965 *J. chem. Phys.* **42**, 3241.
Monchick, L., Yun, K. & Mason, E. A. 1963 *J. chem. Phys.* **39**, 654.
Patankar, S. V. & Spalding, D. B. 1970 *Heat and mass transfer in boundary layers* (2nd edn). London: Intertex Books.
Prescott, R., Hudson, R. L., Foner, S. N. & Avery, W. H. 1954 *J. chem. Phys.* **22**, 145.
Scholte, T. G. & Vaags, P. B. 1959*a* *Combust. Flame* **3**, 495.
Scholte, T. G. & Vaags, P. B. 1959*b* *Combust. Flame* **3**, 503.
Scholte, T. G. & Vaags, P. B. 1959*c* *Combust. Flame* **3**, 511.
Spalding, D. B. & Stephenson, P. L. 1971 *Proc. R. Soc. Lond.* A **324**, 315.
Spalding, D. B., Stephenson, P. L. & Taylor, R. G. 1971 *Combust. Flame* **17**, 55.
Stephenson, P. L. & Taylor, R. G. 1973 *Combust. Flame* **20**, 231.
Svehla, R. A. 1962 *NASA tech. Rep.* R-132.
Tsatsaronis, G. 1978 *Combust. Flame* **33**, 217.
Vandooren, J., Peeters, J. & van Tiggelen, P. J. 1975 *15th Int. Symp. Combust.*, p. 745. Pittsburgh: Combustio Institute.
Walkauskas, P. & Kaufman, F. 1975 *15th Int. Symp. Combust.*, p. 691. Pittsburgh: Combustion Institute.
Wang Chang, C. S., Uhlenbeck, G. E. & de Boer, J. 1964 *Studies in statistical mechanics* (ed. J. de Boer & G. E Uhlenbeck), vol. 2. New York: John Wiley.
Washida, N., Martinez, R. J. & Bayes, K. D. 1974 *Z. Naturf.* A **29**, 251.
Wires, R., Watermeier, L. A. & Strehlow, R. A. 1959 *J. phys. Chem.* **63**, 989.

PHILOSOPHICAL TRANSACTIONS OF THE ROYAL SOCIETY A MATHEMATICAL, PHYSICAL & ENGINEERING SCIENCES